
VALIDATION OF NEURAL NETWORK CONTROLLERS FOR UNCERTAIN SYSTEMS THROUGH KEEP-CLOSE APPROACH: ROBUSTNESS ANALYSIS AND SAFETY VERIFICATION

A PREPRINT

Abdelhafid Zenati*

Department of Engineering,
School of Mathematics, Computer Science and Engineering,
City, University of London Northampton Square,
London, UK, EC1V 0HB.
adelhafid.zenati@city.ac.uk

Nabil Aouf

School of Mathematics, Computer Science and Engineering,
City, University of London Northampton Square,
London, UK, EC1V 0HB.
nabil.aouf@city.ac.uk

David Sanchez de la Llana

European Space Research and Technology Centre,
ESA, 2201 AZ Noordwijk, The Netherlands.
david.sanchez.de.la.llana@esa.int

Samir Bennani

European Space Research and Technology Centre,
ESA, 2201 AZ Noordwijk, The Netherlands.
samir.bennani@esa.int

July 25, 2023

ABSTRACT

Among the major challenges in neural control system technology is the validation and certification of the safety and robustness of neural network (NN) controllers against various uncertainties including unmodelled dynamics, nonlinearities, and time delays. One way in providing such validation guarantees is to maintain the closed-loop system output with a NN controller when its input changes within a bounded set, close to the output of a robustly performing closed-loop reference model. This paper presents a novel approach to analysing the performance and robustness of uncertain feedback systems with NN controllers. Due to the complexity of analysing such systems, the problem is reformulated as the problem of dynamical tracking errors between the closed-loop system with a neural controller and an ideal closed-loop reference model. Then, the approximation of the controller error is characterised by adopting the differential mean value theorem (DMV) and the Integral Quadratic Constraints (IQCs) technique. Moreover, the Relative Integral Square Error (RISE) and the Supreme Square Error (SSE) bounded set are derived for the output of the error dynamical system. The analysis is then performed by integrating Lyapunov theory with the IQCs-based technique. The resulting worst-case analysis provides the user a prior knowledge about the worst case of RISE and SSE between the reference closed-loop model and the uncertain system controlled by the neural controller. By applying the novel approach presented in this paper to two different problems, the theoretical results have been validated. The first problem, the Single-Link Robot Arm Control Problem, focused on a single output, while the second problem, the Deep Guidance and Control of Apollo Lander, dealt with multiple outputs. As a result of these practical tests, the proposed approach has proven to be effective and applicable to various scenarios.

*The main author

Keywords NN Controller · Lyapunov · IQCs · Robustness Analysis · Safety and Verification.

1 Introduction

Neural networks (NNs) show great performances when adopted for tasks where Artificial Intelligence (AI) based solutions are considered. Due to the latest advancements in AI, stabilising dynamical systems with NN controllers is invigorated [Schulman et al., 2015, Pauli et al., 2022]. However, feedback systems with NN controllers still suffer from a lack of robustness, safety certificates and, validation due to their complex, opaque, and large-scale nature structures [Fazlyab et al., 2020, Deka et al., 2022]. Particularly, NN controllers have many types of nonlinear activation functions [Yin et al., 2021b] in addition to their vulnerability to adversarial attacks and system uncertainties [Szegedy et al., 2013, Zheng et al., 2016]. These drawbacks make the application of classical stability analysis methods such as Lyapunov theory to NN controller-based closed-loop systems difficult. This leads to limited adoption of NN controllers in safety-critical applications [Khalil, 2015, Xiang et al., 2018a].

Over the course of the last three decades, the framework of uncertain system systematic analysis via Integral Quadratic Constraints (IQCs) was developed and used [Megretski and Rantzer, 1997, Veenman and Scherer, 2013]. The IQCs approach is proven to be efficient in capturing the properties of various classes of uncertainties such as slope-restricted nonlinearities, dynamics that can not be modeled, and time delays in addition to systems' nonlinearities [Lessard et al., 2016, Veenman et al., 2016]. The flexibility of the approach and its generality made it one of the most important techniques utilized to perform and assess an uncertain dynamical system's stability analysis and performance, respectively [Wang and Manchester, 2019]. In [Iannelli et al., 2019], the problem of stability analysis of nonlinear uncertain systems is formulated using the definition of the augmented plant via the state-space factorization of the IQC. The certificates for the region of attraction are established with both soft and hard IQC factorizations. Then, the formulated problem is solved using a numerical approach such as Sum of Squares (SOS). Based on solving Linear Matrix Inequalities (LMIs), [Fetzer et al., 2017] proposes a novel dynamic multipliers-dependent shift of the Kalman-Yakubovich-Popov (KYP) [Rantzer, 2015] certificate that is expressed using constraints. The novel multipliers allow the formulation of the regional stability properties within IQCs theory, the verification of output constraints and the hard time-domain state. [Summers and Packard, 2010] derives the certification conditions for local \mathcal{L}_2 gain of locally stable interconnected systems. Using estimation of reachability, the approach enhances the local \mathcal{L}_2 gain calculation. Therefore, a set of local (IQCs) can be established for a fixed nonlinear dynamical system. Then by the local IQCs, a local \mathcal{L}_2 gain is obtained. The possibility of using IQCs in the analysis systems subject to saturated linear feedback and the design of its control is the objective of the work in [Fang et al., 2008]. The research there focuses on establishing a IQCs-based conditions set under which an ellipsoid is contractively invariant for such a system. The paper results show that these set invariant conditions are necessary for such a study.

Several formal verification methods recently propose to investigate the stability of closed-loop systems interconnected with NN controllers. In [Xiang et al., 2018b], the authors study the verification problems for a class of piece-wise linear systems with NN controllers. By making an extension to the reachable set estimation, a reduction of the safety verification is established to check for empty junctions between unsafe regions and the reachable set. In [Ivanov et al., 2020], converting the NN controller into a hybrid system equivalent to the original one, the work addresses the issue of safety guarantees for autonomous systems with NN controllers. Moreover, the scalability of the proposed approach using Taylor series approximation with worst-case error bounds is looked at. Using a similar approach as [Ivanov et al., 2020], the work in [Ivanov et al., 2021] emphasizes on NNs with both tanh and sigmoid activation functions. Through the Taylor model preconditioning and shrink wrapping, a Taylor-model-based reachability algorithm is developed and a parallel implementation is provided. [Yin et al., 2021a] presents an approach, which permits the closed loop system with NN controllers to involve different types of perturbations by using IQCs technique and to capture their input/output dynamical behavior.

In this paper, we aim at certifying the safety and providing robustness guarantees for NN controllers against various systems uncertainties including unmodelled dynamics, slope-restricted non-linearities, and time delays. Inspiring from comparison principle [Nam et al., 2021, et al., 2022], the core idea of this work is to provide guarantees in maintaining the output of the uncertain system with a trained NN controller close to an ideal reference closed-loop model when its inputs change within a bounded set. To this end, a novel approach to analyse the dynamical error stability of the feedback system with a NN controller and a reference closed-loop model is presented. Since analysing such systems is complicated, the problem is reformulated as the dynamical tracking errors between the uncertain interconnected system with a NN and the reference closed-loop model. Approximation of the neural controller error is then performed using the differential mean value theorem (DMV) and integral quadratic constraints (IQCs) in order to eliminate the neural controller's nonlinearity. As the time integral of the square of the error (ISE) is used to evaluate the system's performance [Atkins et al., 2013], the RISE and SSE bounded sets are derived based on generating dissipation-inequality conditions. These conditions of the RISE and SSE bound the worst-case $\mathcal{L}_2 \rightarrow \mathcal{L}_2$ and $\mathcal{L}_2 \rightarrow \mathcal{L}_\infty$ induced gain of

the dynamical error system, respectively. In addition, Lyapunov theory is integrated with IQCs-based techniques to accomplish the analysis of the worst-case gains. This analysis determines the worst-case ISE between the closed-loop reference model and the neural-controlled uncertain system. Using the difference between the closed-loop reference system and interconnected system with a NN is an appealing approach for the following reasons: (i) it can eliminate the non-linearity of the NN controller by applying the Differential Mean Value theorem which is more suitable and easier to analyse. (ii) The work in [Pfifer and Seiler, 2015] considered the trivial initial conditions to facilitate the analysis. However, these conditions limit the application of their results to real challenging problems. Indeed, in the real world, the initial condition has a big effect on the stability of the system and generally, it is not null. Our keep-close technique can function on any initial condition of the system. Using the difference between the closed-loop reference system and the interconnected system with a NN controller, the initial conditions become null which makes the analysis easier, plausible, and more general. In [Fazlyab et al., 2020], the authors analysed the stability of feedback systems with NN controllers using IQCs approach to capture their input/output behavior. Their theoretical result relies on semi-definite programming to estimate the Attraction Region (ROA) of the equilibrium point. Our keep-close approach is more general as it covers the tracking in general where the convergence to an equilibrium point is a particular case. Moreover, from verification and safety point of view, the keep-close approach is more practical than the result in [Fazlyab et al., 2020] because it can indicate the occurrence likelihood of any undesirable behavior before the convergence to the equilibrium point. The novel approach outlined in this paper has been implemented and tested in practice. Validation was carried out on two specific problems: the Single-Link Robot Arm Control Problem, which focused on a single output scenario, and the Deep Guidance and Control of Apollo Lander, which dealt with multiple outputs. These tests provide empirical support for the efficacy and adaptability of the proposed approach across different application domains.

The rest of this paper is organized as follows: The problem formulation and preliminaries are given in Section 2. Section 3 is devoted to the robustness analysis when the system is submitted to uncertainties. In Section 3, a numerical example is provided to illustrate the results of our proposed solution. Conclusions are given in Section 4.

1.1 Notation

- \mathbb{R} , \mathbb{R}_+ , and \mathbb{C} refer to the set of real, non-negative real, and complex numbers, respectively. Also, in the complex plane, the notation \mathbb{RH} denote to all analytic functions within the closed exterior of the unit disk. M^T and M^* are the transpose and complex conjugate transpose of the matrix M , respectively.
- Consider the LPV system Σ where its matrices of state space depend on a time-varying parameter vector $s(t) : \mathbb{R}_+ \rightarrow \mathcal{S}$ and $\mathcal{S} \subset \mathbb{R}^n$. $s(t)$ a continuously differentiable function of time where the parameter rates of variation $\dot{s}(t) : \mathbb{R}_+ \rightarrow \dot{\mathcal{S}}$. $\dot{\mathcal{S}}$ is a hyperrectangle given by:

$$\dot{\mathcal{S}} = \left\{ \rho \in \mathbb{R}^n \mid \underline{\rho}_i \leq \rho_i \leq \bar{\rho}_i, i = 1 \cdots n \right\} \quad (1)$$

Let a parameter-dependent matrix P a continuously differentiable function of the parameter s given by: $P : \mathcal{S} \rightarrow \mathbb{S}^n$, \mathbb{S}^n refers to the set of $n \times n$ symmetric matrices. The differential operator $\partial P : \mathcal{S} \times \dot{\mathcal{S}} \rightarrow \mathbb{S}^n$ is given by:

$$\partial P(s, \dot{s}) = \sum_{k=1}^n \frac{\partial P(s)}{\partial s_k} \dot{s}_k \quad (2)$$

- The space \mathcal{L}_2 denotes the set of functions $\varphi : \mathbb{R}_+ \rightarrow \mathbb{R}^n$ satisfying $\|\varphi\|_2 < \infty$

$$\|\varphi\|_2 = \left[\int_0^{+\infty} \varphi(\tau)^T \varphi(\tau) d\tau \right]^{\frac{1}{2}} \quad (3)$$

- The space \mathcal{L}_∞ refers to the set of functions $\varphi : \mathbb{R}_+ \rightarrow \mathbb{R}^n$ satisfying $\|\varphi\|_\infty < \infty$

$$\|\varphi\|_\infty = \sup_{t \in [0, \infty)} [\varphi(t)^T \varphi(t)]^{\frac{1}{2}} \quad (4)$$

- We recall here the Differential Mean Value (DMV) Theorem:

Lemma 1 (DMV Theorem [Zemouche et al., 2005, Sharma et al., 2016]) *Let $y_1, y_2, x \in \mathbb{R}^n$ and $\Upsilon : \mathbb{R}^n \rightarrow \mathbb{R}^m$ be a continuous and differentiable function on convex hull of the set $\text{Co}(y_1, y_2)$. Then, there are constant vectors $s_1, \dots, s_m \in \text{Co}(y_1, y_2)$, $s_i \neq y_1$, $s_i \neq y_2$, $i = 1, \dots, m$ such that:*

$$\Upsilon(y_1) - \Upsilon(y_2) = \left(\sum_{i=1}^m \sum_{j=1}^n e_m(i) e_n^T(j) \frac{\partial \Upsilon_i}{\partial x_j}(s_i) \right) (y_1 - y_2) \quad (5)$$

where $\text{Co}(y_1, y_2) = \alpha y_1 + (1 - \alpha)y_2, 0 \leq \alpha \leq 1$ is the convex domain of y_1, y_2 and $e_m(i)$ is a the canonical basis vector of \mathbb{R}^m with 1 at i -th component with

$$e_m(i) = (0, \dots, 0, 1, 0, \dots, 0)^T \in \mathbb{R}^m \quad (6)$$

- As the aim in this work is to estimate the Integral Square Error (ISE) and worst expected Supreme Square Error (SSE), it is worth to define those metrics as following:

Definition 1 (RISE & SSE) Let us consider y and \hat{y} are the outputs of the closed-loop interconnected-based NN system and the closed-loop reference model, respectively. Then the Relative Integral Square Error (RISE) and the Supreme Square Error (SSE) are given by :

$$RISE \triangleq \frac{\|y - \hat{y}\|_2}{\sqrt{\|y\|_2^2 + \|\hat{y}\|_2^2}}, \quad SSE \triangleq \frac{\|y - \hat{y}\|_\infty}{\sqrt{\|y\|_2^2 + \|\hat{y}\|_2^2}} \quad (7)$$

where the worst case of the Relative Integral Square Error γ and the worst case of the Supreme Square Error σ satisfy:

$$\frac{\|y - \hat{y}\|_2}{\sqrt{\|y\|_2^2 + \|\hat{y}\|_2^2}} \leq \gamma, \quad \frac{\|y - \hat{y}\|_\infty}{\sqrt{\|y\|_2^2 + \|\hat{y}\|_2^2}} \leq \sigma \quad (8)$$

2 Problem formulation

2.1 Keep-Close Approach

A robustness analysis of feedback systems based on NN controllers against potential uncertainties is presented here. To achieve this, the output of the closed-loop system with a NN controller is kept close to the output of an ideal and trusted closed-loop reference model when its input changes within a bounded set. Consider the closed-loop interconnected-based NN system with the uncertainty Δ in Figure 1, (i.e. the uncertain plant $F(P, \Delta)$ and NN π). The perturbed plant $F(P, \Delta)$ is an interconnection of a nominal plant P and an uncertainty Δ which can be described mathematically by the following dynamical equations:

$$\Sigma_{F(P, \Delta)}^\pi := \begin{cases} \dot{x}(t) = Ax(t) + Bu(t) + \tilde{B}q_\delta(t) \\ y(t) = Cx(t) + Du(t) + \tilde{D}q_\delta(t) \\ q_\delta(t) = \Delta(p_\delta(t) = y(t)) \\ u(t) = \pi(y(t)) \in \mathcal{L}_2 \\ x(0) = x_0 \end{cases} \quad (9)$$

where $x \in \mathbb{R}^n$ is the system's state vector, control inputs of the neural controller $u \in \mathbb{R}^m$ and $(A, B, C, D, \tilde{B}, \tilde{D})$ are known, and the perturbation operator Δ is a bounded, causal. In this study, we aim to ensure that the closed-loop system with a NN controller $\Sigma_{F(P, \Delta)}^\pi$ keeps its outputs close to a given reference model $\Sigma_{Ref}^{\pi^*}$ (a closed-loop system with an ideal, and classically proven controller). This reference model can be given by:

$$\Sigma_{Ref}^{\pi^*} := \begin{cases} \dot{\hat{x}}(t) = A\hat{x}(t) + B\hat{u}(t) \\ \hat{y}(t) = C\hat{x}(t) + D\hat{u}(t) \\ \hat{u}(t) = \pi^*(\hat{y}(t), t) \in \mathcal{L}_2 \\ \hat{x}(0) = x_0 \end{cases} \quad (10)$$

with reference system's state vector $\hat{x} \in \mathbb{R}^n$, control inputs $\hat{u} \in \mathbb{R}^m$ and (A, B, C, D) known as it is mentioned in (9). To accomplish our aim stated above, an analysis of the dynamical error system between the two closed-loop systems (i.e. the reference model and the system closed with a NN controller) is presented in the following section. We start by mathematically describing the dynamical error system. Let us assume that the state of dynamical error system is given by $\zeta(t) = x(t) - \hat{x}(t)$ and $z(t) = p_\delta(t) - \hat{y}(t)$, then, $\dot{\zeta}(t) = \dot{x}(t) - \dot{\hat{x}}(t)$, where

$$\Sigma_{\tilde{F}(\tilde{P}, \Delta)}^\mu := \begin{cases} \dot{\zeta}(t) = A\zeta(t) + B\mu(t) + \tilde{B}q_\delta(t) \\ z(t) = C\zeta(t) + D\mu(t) + \tilde{D}q_\delta(t) \\ \mu(t) = \pi(y(t)) - \pi^*(\hat{y}(t), t) \\ \zeta(0) = 0 \end{cases} \quad (11)$$

where $\mu(t)$ is the approximation of the controller error (between the NN controller and the ideal controller adopted in the closed loop reference model). Also, the initial condition of the dynamical error state $\zeta(t)$ is $\zeta(0) = 0$ because $x(0) = \hat{x}(0) = x_0$.

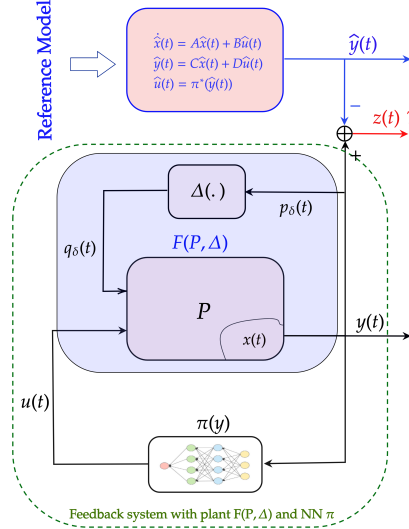


Figure 1: Feedback system with plant $F(P, \Delta)$ and NN π with closed loop Reference Model.

2.2 Integral Quadratic Constraints (IQCs) Concept

The key concept of IQCs is instead of investigating the dynamical behaviour of the system that contains uncertainty Δ , we analyze the system where Δ is removed and the signals $(p(t), q(t))$ are utilized to enforce the following constraints:

$$\int_{-\infty}^{+\infty} \begin{bmatrix} \hat{p}(j\omega) \\ \hat{q}(j\omega) \end{bmatrix}^* \Pi(j\omega) \begin{bmatrix} \hat{p}(j\omega) \\ \hat{q}(j\omega) \end{bmatrix} d\tau \geq 0 \quad (12)$$

where $\Pi(j\omega)$ is named an ‘‘IQC multiplier’’ or can simply called a ‘‘multiplier’’, $\hat{p}(j\omega)$ and $\hat{q}(j\omega)$ are Fourier transforms of $p(t)$ and $q(t)$, respectively. Since (12) is valid for all admissible choices of Δ , then all properties can be proved for the constrained system are hold also for the original system. Therefore, the mathematical relationship between input-output quantities of system components can be described via IQCs. The IQC in (12) can be described in the time domain based on Parseval Theorem [Kelkar et al., 1983]. Assuming that Π is function that is uniformly bounded and rational. Then, $\Pi(j\omega)$ can be factorized as:

$$\Pi(j\omega) = \Psi(j\omega)^* \mathcal{M} \Psi(j\omega), \quad (13)$$

where $\Psi(j\omega) \in \mathbb{RH}$ and \mathcal{M} represents a constant matrix [Veenman et al., 2016]. $\Psi(j\omega)$ is expressed as:

$$\Psi(j\omega) := C_\Psi j[\omega I - A_\Psi] \begin{bmatrix} B_{\Psi 1} & B_{\Psi 2} \end{bmatrix} + \begin{bmatrix} D_{\Psi 1} & D_{\Psi 2} \end{bmatrix} \quad (14)$$

Then, the IQC of (12) can be written as:

$$\int_0^{+\infty} r(\tau)^T \mathcal{M} r(\tau) d\tau \geq 0 \quad (15)$$

where $r(t)$ is the output of the following linear system:

$$\Psi := \begin{cases} \dot{\psi}(t) & = A_\Psi \psi(t) + B_{\Psi 1} p(t) + B_{\Psi 2} q(t) \\ r(t) & = C_\Psi \psi(t) + D_{\Psi 1} p(t) + D_{\Psi 2} q(t) \\ \psi(0) & = 0 \end{cases} \quad (16)$$

The time-domain constraint (17) is generally satisfied over infinite time intervals. A hard IQC satisfies the following more restrictive conditions: If Δ is any causal and bounded operator that fulfills (12) then:

$$\int_0^T r(\tau)^T \mathcal{M}r(\tau) d\tau \geq 0 \quad (17)$$

holds for all $T \geq 0$. Conversely, the soft IQCs in the time-domain constraint do not require to hold overall finite time intervals. This property is critical because the major technical and pedagogical problems in the IQCs framework occur when we utilize soft IQCs. Unfortunately, there is an ambiguity surrounding both terms soft IQC and hard IQC. Particularly, the unicity of factorization of $\Pi(j\omega)$ as $\Psi^*(j\omega)\mathcal{M}\Psi(j\omega)$, is not unique. For clarity, the following definition will be adopted in the rest of the paper.

Definition 2 (Hard IQC [Pfifer and Seiler, 2015]) *A uniformly bounded and rational function $\Pi : j\mathbb{R} \rightarrow \mathbb{C}$ admits a hard IQC factorization if there exists $\Psi(j\omega) \in \mathbb{RH}$ and matrix \mathcal{M} with $\mathcal{M}_{ij} \in \mathbb{C}$, such that $\Pi(j\omega) = \Psi^*(j\omega)\mathcal{M}\Psi(j\omega)$, and any bounded, causal operator Δ which satisfies the IQC defined by $\Pi(j\omega)$ also satisfies:*

$$\int_0^T r(\tau)^T \mathcal{M}r(\tau) d\tau \geq 0 \quad (18)$$

for all $T \geq 0$ and for all $p(t) \in \mathcal{L}_2([0, \infty))$, $q = \Delta(p)$. $(\Psi(j\omega), \mathcal{M})$ is a hard IQCs factorization of Π .

2.3 Controller Error Analysis

This subsection analyses the approximation of the controller error $\mu(t)$ (i.e. the difference between the NN controller and the ideal controller adopted in the reference closed-loop model). The objective of this analysis is to find a less conservative and better representative expression of $\mu(t)$ where we can extract and dissociate certain and uncertain quantities from $\mu(t)$. Then, this expression can be directly used in the dynamic error system (11). To reach the objective mentioned above let us start by introducing the following lemma:

Lemma 2 (Controller Error) *Consider the dynamics of the error in (11) and the bounded NN controller π , the approximation error $\mu(t)$ given in (11) can be expressed as:*

$$\mu(t) = [I - \Lambda(s)D]^{-1} [\Lambda(s)C\zeta(t) + \Lambda(s)\tilde{D}\Delta(y(t)) + \epsilon(\hat{y}(t))] \quad (19)$$

if $D = 0$, therefore

$$\mu(t) = \Lambda(s)C\zeta(t) + \Lambda(s)\tilde{D}\Delta(y(t)) + \epsilon(\hat{y}(t)) \quad (20)$$

and the vectors $s_1, \dots, s_n \in \mathbf{Co}(y(t), \hat{y}(t))$, $s_i \neq y_1$, $s_i \neq y_2$, $i = 1, \dots, n$ such that

$$\Lambda(s) = \sum_{i=1}^m \sum_{j=1}^n e_m(i) e_n^T(j) \frac{\partial \pi_i}{\partial y_j}(s_i) \quad (21)$$

where $e_m(i) = (0, \dots, 0, 1, 0, \dots, 0)^T \in \mathbf{R}^m$ is a canonical basis vector of \mathbf{R}^m with 1 at i -th component.

Proof: From (11), the error approximation $\mu(t)$ is given by:

$$\mu(t) = \pi(y(t)) - \pi^*(\hat{y}(t), t) \quad (22)$$

Adding and subtracting $\pi(\hat{y}(t))$, the error approximation $\mu(t)$ can be expressed by:

$$\begin{aligned} \mu(t) &= \pi(y(t)) - \pi^*(\hat{y}(t), t) + \pi(\hat{y}(t)) - \pi(\hat{y}(t)) \\ &= \pi(y(t)) - \pi(\hat{y}(t)) + \epsilon(\hat{y}(t)) \end{aligned} \quad (23)$$

where the trained NN controller error $\epsilon(y(t))$ given by:

$$\epsilon(\hat{y}(t)) = \pi(\hat{y}(t)) - \pi^*(\hat{y}(t), t) \quad (24)$$

On the other hand, using the Differential Mean Value Theorem in lemma 1 and the fact that the function π is continuous and differentiable on convex hull of the set $\mathbf{Co}(y(t), \hat{y}(t))$, then, there are vectors $s_1, \dots, s_n \in \mathbf{Co}(y(t), \hat{y}(t))$, $s_i \neq y$, $s_i \neq \hat{y}$, $i = 1, \dots, n$. Because $z(t) = C\zeta(t) + D\mu(t) + \tilde{D}q_\delta(t)$, then

$$\begin{aligned} \pi(y(t)) - \pi(\hat{y}(t)) &= \Lambda(s)(y(t) - \hat{y}(t)) = \Lambda(s)z(t) \\ &= \Lambda(s) [C\zeta(t) + D\mu(t) + \tilde{D}q_\delta(t)] \end{aligned} \quad (25)$$

where

$$\Lambda(s) = \sum_{i=1}^m \sum_{j=1}^n e_m(i) e_n^T(j) \frac{\partial \pi_i}{\partial x_j}(s_i), \quad q_\delta(t) = \Delta(y(t))$$

The equations (23) and (25) allow us to conclude that:

$$\mu(t) = [I - \Lambda(s)D]^{-1} [\Lambda(s)C\zeta(t) + \Lambda(s)\tilde{D}q_\delta(t) + \epsilon(\hat{y}(t))] \quad (26)$$

where $\epsilon(\hat{y}(t)) = \pi(\hat{y}(t)) - \pi^*(\hat{y}(t), t)$.

□

During the design of a control system, the feed-through matrix D can be adjusted to achieve desired control objectives and ensure that $I - \Lambda(s)D$ is invertible. Control strategies and the desired impact of inputs on outputs, in conjunction with state feedback control, determine whether the feed-through matrix is nonzero or zero. The feed-through matrix D is usually a zero matrix, i.e. $D = 0$.

The result of (19) represents less conservative and better representative expression of $\mu(t)$. The certain quantity $\Lambda(s)C\zeta(t)$ depends on the weights of the neural controller and the state of the dynamical error system $\zeta(t)$ which is similar to what we call within the control theory community as state-feedback control. For the uncertain quantities, we have two terms $\Lambda(s)D_p\Delta(y(t))$ and $\epsilon(\hat{y}(t))$ depending on the outputs of the interconnected system with a NN controller and the closed loop reference model, respectively. The term $\Lambda(s)D_p\Delta(y(t))$ represents the effect of the uncertainty of the plant on the controller whereas the term $\epsilon(\hat{y}(t))$ illustrates the training error effect on the dynamical error system which is very small and bounded because the purpose of the training is to minimize this quantity $|\epsilon(\hat{y}(t))|$.

2.4 IQCs Characteristics of Uncertainties

The perturbation acting on the feedback system can represent diverse types of uncertainty, such as unmodeled dynamics, saturation, time delay, and slope-restricted nonlinearities. Knowing that the term $\epsilon(\hat{y}(t)) = \pi(\hat{y}(t)) - \pi^*(\hat{y}(t), t)$ represents the training error which is very small and bounded because the purpose of the training is to minimize this quantity $\min |\epsilon(\hat{y}(t))|$. Also, the input-output relationship of the uncertainties $\Delta(\cdot)$ can be mathematically described, as (18), by integral quadratic constraints (IQCs). Accordingly, the IQCs technique can be adopted to characterise the uncertainties $\epsilon(\cdot)$ and $\Delta(\cdot)$. This later leads to the following assumption:

Assumption 1 Assume that the outputs of the closed-loop reference model and the closed-loop reference system and the interconnected system with a NN controller $\hat{y}(t) = p_\epsilon(t) \in \mathcal{L}_2$ and $y(t) = p_\delta(t) \in \mathcal{L}_2$, having bounded, causal operators $\Delta(\cdot)$ and $\epsilon(\cdot)$ which satisfy the IQCs defined by $\Pi_\epsilon(j\omega)$ and $\Pi_\delta(j\omega)$, respectively. The input-output relationship of the uncertainties $\Delta(\cdot)$ and $\epsilon(\cdot)$ can be mathematically described, as (18), by integral quadratic constraints (IQCs) as follows: :

$$\begin{cases} \int_0^T r_\delta(\tau)^T \mathcal{M}_\delta r_\delta(\tau) d\tau \geq 0 \\ \int_0^T r_\epsilon(\tau)^T \mathcal{M}_\epsilon r_\epsilon(\tau) d\tau \geq 0 \end{cases} \quad (27)$$

for all $T \geq 0$ and for all $\hat{y}(t), y(t) \in \mathcal{L}_2([0, \infty))$. $(\Psi_\epsilon(j\omega), \mathcal{M}_\epsilon)$ and $(\Psi_\delta(j\omega), \mathcal{M}_\delta)$ are a hard IQCs factorization of Π_ϵ and Π_δ , respectively.

Corollary 1 Consider Assumption 1, the signals $r_\delta(t)$ and $r_\epsilon(t)$ in (27) are the output of the following LTI systems, respectively:

$$\Psi_\delta := \begin{cases} \dot{\psi}_\delta(t) &= A_\delta \psi_\delta(t) + B_{\delta 1} q_\delta(t) + B_{\delta 2} p_\delta(t) \\ r_\delta(t) &= C_\delta \phi(t) + D_{\delta 1} q_\delta(t) + D_{\delta 2} p_\delta(t) \\ \psi_\delta(0) &= 0 \end{cases} \quad (28)$$

and

$$\Psi_\epsilon := \begin{cases} \dot{\psi}_\epsilon(t) &= A_\epsilon \psi_\epsilon(t) + B_{\epsilon 1} q_\epsilon(t) + B_{\epsilon 2} p_\epsilon(t) \\ r_\epsilon(t) &= C_\epsilon \phi(t) + D_{\epsilon 1} q_\epsilon(t) + D_{\epsilon 2} p_\epsilon(t) \\ \psi_\epsilon(0) &= 0 \end{cases} \quad (29)$$

where Ψ_δ and Ψ_ϵ represent the ‘virtual’ filters as in (16) applied to the inputs p_δ and p_ϵ and outputs q_δ and q_ϵ of Δ and ϵ and a constraint on the outputs r_δ and r_ϵ of (16). Thus, an extended filter can be written as follows:

$$\Xi := \begin{cases} \dot{\xi}(t) &= A_\xi \xi(t) + B_{\xi 1} q(t) + B_{\xi 2} p(t) \\ r(t) &= C_\xi \xi(t) + D_{\xi 1} q(t) + D_{\xi 2} p(t) \\ \xi(0) &= 0 \end{cases} \quad (30)$$

where

$$\xi(t) = \begin{bmatrix} \psi_\delta(t) \\ \psi_\epsilon(t) \end{bmatrix}, \quad p(t) = \begin{bmatrix} p_\delta(t) \\ p_\epsilon(t) \end{bmatrix}, \quad q(t) = \begin{bmatrix} q_\delta(t) \\ q_\epsilon(t) \end{bmatrix}$$

and the matrices of (30) are defined as follow:

$$A_\xi = \begin{bmatrix} A_\delta & 0 \\ 0 & A_\epsilon \end{bmatrix}, \quad B_{\xi 1} = \begin{bmatrix} B_{\delta 1} & 0 \\ 0 & B_{\epsilon 1} \end{bmatrix}, \quad B_{\xi 2} = \begin{bmatrix} B_{\delta 2} & 0 \\ 0 & B_{\epsilon 2} \end{bmatrix} \\ C_\xi = \begin{bmatrix} C_\delta & 0 \\ 0 & C_\epsilon \end{bmatrix}, \quad D_{\xi 1} = \begin{bmatrix} D_{\delta 1} & 0 \\ 0 & D_{\epsilon 1} \end{bmatrix}, \quad D_{\xi 2} = \begin{bmatrix} D_{\delta 2} & 0 \\ 0 & D_{\epsilon 2} \end{bmatrix}$$

3 Robust Tracking Analysis via Standard IQCs

Considering the error dynamics system of (11), the conservative expression of the μ in (20), and let $\chi(t) = [\zeta(t) \ \xi(t)]^T$ be the extended average state vector with dynamics given by the following (omitting s for a shorter notation):

$$\Sigma_{ex} \begin{cases} \dot{\chi}(t) &= \mathcal{A}\chi(t) + \mathcal{B}_1 q(t) + \mathcal{B}_2 \eta(t) \\ r(t) &= \mathcal{C}_1 \chi(t) + \mathcal{D}_{11} q(t) + \mathcal{D}_{12} \eta(t) \\ z(t) &= \mathcal{C}_2 \chi(t) + \mathcal{D}_{21} q(t) + \mathcal{D}_{22} \eta(t) \\ \eta(t) &= [y^T(t) \ \hat{y}^T(t)]^T, \quad \chi(0) = 0 \end{cases} \quad (31)$$

where the matrices of the Linear Parameter Varying (LPV) extended system (31) have the appropriate dimensions.

$$\mathcal{A}(s) = \begin{bmatrix} A + B [I - \Lambda(s)D]^{-1} \Lambda(s)C & 0 \\ 0 & A_\xi \end{bmatrix} \\ \mathcal{B}_1(s) = \begin{bmatrix} B [I - \Lambda(s)D]^{-1} \Lambda(s) \tilde{D} + \tilde{B} & B \\ B_{\delta 2} & 0 \\ 0 & B_{\epsilon 2} \end{bmatrix}, \quad \mathcal{B}_2 = \begin{bmatrix} 0 \\ B_\xi \end{bmatrix} \\ \mathcal{C}_1 = \begin{bmatrix} 0 \\ C_\xi \end{bmatrix}, \quad \mathcal{C}_2(s) = \begin{bmatrix} C + D [I - \Lambda(s)D]^{-1} \Lambda(s)C & 0 \\ 0 & 0 \end{bmatrix} \\ \mathcal{D}_{11} = \begin{bmatrix} 0 \\ D_{\xi 2} \end{bmatrix}, \quad \mathcal{D}_{12} = \begin{bmatrix} 0 \\ D_{\xi 2} \end{bmatrix}, \quad \mathcal{D}_{22} = 0 \\ \mathcal{D}_{21}(s) = \begin{bmatrix} \tilde{D} + D [I - \Lambda(s)D]^{-1} \Lambda(s) \tilde{D} & D [I - \Lambda(s)D]^{-1} \\ 0 & 0 \end{bmatrix}, \quad (32)$$

This extended system is obtained using the dynamics error system of (11). According to [Pfifer and Seiler, 2015], the approximation error $\mu(t)$ expression in (19), and the extended virtual filter (30). The new system (31) is equivalent to Fig. 2, where the system has an input of the state of the uncertain system $\eta(t)$ and its output is the output of the error $z(t)$ with the uncertainties Δ and ϵ , see Fig. 2. In the other hand, a dissipation inequality can be formulated to upper bound the worst-case \mathcal{L}_2 gain of $\tilde{F}(\tilde{P}, \Delta, \epsilon)$ of Fig. 2 utilizing the extended system (31) and the time domain IQCs (27).

3.1 Relative Integral Square Error (RISE)

The following theorem derives the conditions for the worst case Relative Integral of the Square of the Error (RISE) metric. In control theory, RISE is used to assess the performance of a system [Atkins et al., 2013]. RISE provides valuable information about the behavior of the uncertain closed-loop system with an NN controller compared to the closed-loop reference model.

Theorem 1 (Worst-case of RISE) *Let Δ and ϵ satisfy IQC(Ξ, M) and assume that the extended system Σ_{ex} of (31) is well-posed. If there exists a scalar $\lambda > 0$ and a continuously differentiable matrix $P = P^T$ with appropriate*

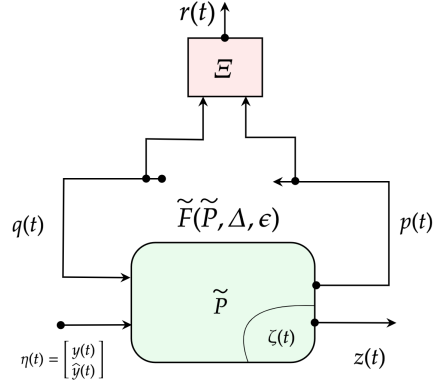


Figure 2: Graphical interpretation of the IQCs with the equivalent system.

dimensions such that $P \geq 0$ and for all $(s, \dot{s}) \in \Omega \times \dot{\mathcal{S}}$ (Omitting s and \dot{s} for a shorter notation):

$$\begin{aligned}
 & \begin{bmatrix} PA + AP^T + \partial P & PB_1 & PB_2 \\ \mathcal{B}_1^T P & 0 & 0 \\ \mathcal{B}_2^T P & 0 & -I \end{bmatrix} \\
 & + \frac{1}{\gamma^2} \begin{bmatrix} \mathcal{C}_2^T \\ \mathcal{D}_{21}^T \\ \mathcal{D}_{22}^T \end{bmatrix} [\mathcal{C}_2 \quad \mathcal{D}_{21} \quad \mathcal{D}_{22}] \\
 & + \lambda \begin{bmatrix} \mathcal{C}_1^T \\ \mathcal{D}_{11}^T \\ \mathcal{D}_{12}^T \end{bmatrix} M [\mathcal{C}_1 \quad \mathcal{D}_{11} \quad \mathcal{D}_{12}] < 0
 \end{aligned} \tag{33}$$

Then,

- the Relative Integral Square Error (RISE) satisfies:

$$\sup_{s \in \Omega} \sup_{0 \neq \eta \in \mathcal{L}_2, \zeta(0)=0} \left[\frac{\|y - \hat{y}\|_2}{\sqrt{\|y\|_2^2 + \|\hat{y}\|_2^2}} \right] \leq \gamma \tag{34}$$

and

$$\|y - \hat{y}\|_2 < \frac{2\gamma}{1 - \gamma} \|\hat{y}(t)\|_2 \tag{35}$$

Proof: Consider the different signals (χ, z, p, η, r) of the error dynamics system in with the input $\eta \in \mathcal{L}_2$ and solution trajectory χ with zero initial conditions $\chi(0) = 0$. Assuming the well-posedness of (31) means that all signals of this system are well-defined. By assumption, the uncertainties Δ and ϵ satisfy the IQC defined by (Ξ, M) , and hence the quantity r must satisfy the IQC time domain (27) for any $T > 0$. Also, using the state space representation of the virtual filter in (16), the quantity $r^T M r$ is expressed as follow:

$$r M r^T = \begin{bmatrix} \xi \\ p \\ q \end{bmatrix}^T \begin{bmatrix} C_\xi^T M C_\xi & C_\xi^T M D_\xi \\ D_\xi^T M C_\xi & D_\xi^T M D_\xi \end{bmatrix} \begin{bmatrix} \xi \\ p \\ q \end{bmatrix} \tag{36}$$

The following proof is based on defining a parameter-dependent storage function or Lyapunov function $V : \mathbb{R}^x \times \Omega \rightarrow \mathbb{R}_+$ given by $V(\chi, s) = \chi^T P(s) \chi$. Clearly, the condition (33) is a strict inequality which implies that there exists very

small quantity $\varepsilon > 0$ such that the following perturbed matrix inequality holds for all $s \in \Omega$:

$$\begin{aligned} & \begin{bmatrix} PA^T + AP^T + \partial P & PB_1 & PB_2 \\ \mathcal{B}_1^T P & 0 & 0 \\ \mathcal{B}_2^T P & 0 & -(1-\varepsilon)I \end{bmatrix} \\ & + \frac{1}{\gamma^2} \begin{bmatrix} \mathcal{C}_2^T \\ \mathcal{D}_{21}^T \\ \mathcal{D}_{22}^T \end{bmatrix} [\mathcal{C}_2 \quad \mathcal{D}_{21} \quad \mathcal{D}_{22}] \\ & + \lambda \begin{bmatrix} \mathcal{C}_1^T \\ \mathcal{D}_{11}^T \\ \mathcal{D}_{12}^T \end{bmatrix} M [\mathcal{C}_1 \quad \mathcal{D}_{11} \quad \mathcal{D}_{12}] \leq 0 \end{aligned} \quad (37)$$

Taking into account (36) and multiplying left and right (37) by $[\chi^T, q^T, \eta^T]$ and its transpose $[\chi^T, q^T, \eta^T]^T$ where we can see that V satisfies the following dissipation inequality:

$$\nabla_{\chi} V \dot{\chi} + \nabla_s V \dot{s} \leq -\frac{1}{\gamma^2} z^T z + (1-\varepsilon) \eta^T \eta - \lambda r M r^T \quad (38)$$

This yields that the dissipation inequality (38) is equivalent to the perturbed linear matrix inequality (33). Clearly, integrating the dissipation inequality gotten in (38) from lower bound time $t = 0$ to upper bound time $t = T$ with the initial condition satisfies $\chi(0) = 0$ to yield:

$$\begin{aligned} & V(\chi(T)) + \lambda \int_0^T r(\tau)^T M r(\tau) d\tau \leq (1-\varepsilon) \\ & \times \int_0^T \eta(\tau) \eta(\tau)^T d\tau - \frac{1}{\gamma^2} \int_0^T z(\tau) z(\tau)^T d\tau \end{aligned} \quad (39)$$

It follows from the positivity condition of IQCs as in (27), $\lambda \geq 0$, and also due to the non-negativity of the storage function V leads to:

$$\frac{1}{\gamma^2} \int_0^T z(\tau) z(\tau)^T d\tau \leq (1-\varepsilon) \int_0^T \eta(\tau) \eta(\tau)^T d\tau \quad (40)$$

As we assume that $\varepsilon > 0$, thus

$$\lim_{T \rightarrow +\infty} \left[\frac{1}{\gamma^2} \int_0^T z(\tau) z(\tau)^T d\tau < \int_0^T \eta(\tau) \eta(\tau)^T d\tau \right] \quad (41)$$

Knowing that

$$\begin{aligned} \|z(t)\|_2 &= \|y(t) - \hat{y}(t)\|_2 \\ \|\eta(t)\|_2 &= \sqrt{\|y(t)\|_2^2 + \|\hat{y}(t)\|_2^2} \end{aligned} \quad (42)$$

this allows us to deduce that:

$$\sup_{s \in \Omega} \sup_{0 \neq y, \hat{y} \in \mathcal{L}_2, \zeta(0)=0} \frac{\|y - \hat{y}\|_2}{\sqrt{\|y\|_2^2 + \|\hat{y}\|_2^2}} \leq \gamma \quad (43)$$

Additionally, the next part of the proof will be based on the following inequalities

$$\begin{aligned} \sqrt{\|y\|_2^2 + \|\hat{y}\|_2^2} &\leq \|y\|_2 + \|\hat{y}\|_2 \\ \|y\|_2 &= \|y - \hat{y} + \hat{y}\|_2 \leq \|y - \hat{y}\|_2 + \|\hat{y}\|_2 \end{aligned} \quad (44)$$

Using (44) and (43), we get

$$\|y - \hat{y}\|_2 < \frac{2\gamma}{1-\gamma} \|\hat{y}(t)\|_2 \quad (45)$$

□ The value γ in Theorem 1 generally represents the largest \mathcal{L}_2 gain overall allowable parameter trajectories. In this case, it gives information about the worst case of the worst case of RISE between the closed loop reference model and the closed-loop system with neural controller under neural

controller parameters Λ and its training error ϵ . This information is valuable as it provides prior knowledge about the behavior of the interconnected plant submitted to the uncertainty Δ . In other words, the result of this theorem can be used to improve the robustness of the NN controller by making the dynamical error smaller which will guarantee a better performance of the NN controller when it is implemented. This worst-case measure is also an indication of the appearance likelihood of any undesirable behavior in the closed-loop system when adopting the designed NN controller.

On the other hand, the equation (35) holds substantial significance as it delineates the correlation between the expected error in a system with neural networks (NN) and the reference model, with the upper limit set by term $\frac{2\gamma}{1-\gamma}$ multiplied by the reference model norm. As a result of this crucial relationship, it is possible to understand how the NN operates and predict the worst-case scenario for the system. As a result of understanding this equation, we can improve risk management as well as fine-tune the system so that deviations from the reference model are minimized.

3.2 Supreme Square Error (SSE)

The Linear Parameter Varying (LPV) model approximation of the robust tracking problem developed above can be further analysed for more conservative conditions. Indeed, LPV robust performance analysis of (31) can be extended to cover less conservative performance measurements than the Relative Integral Square Error (RISE). The following theorem is to derive the condition for worst case of Supreme Square Error (SSE) σ that less conservative conditions as $\|y - \hat{y}\|_2 \geq \|y - \hat{y}\|_\infty$. More precisely than RISE, SSE provides significant information about the dynamical behavior of the interconnected system with a NNs controller compared to the closed-loop reference model. Based on the definition 1, SSE is a good estimation for the maximum error between the two systems' outputs. If the user can find the bound set of the SSE which leads to increase the level of the truest for the user to adopt these schemes.

Theorem 2 (Worst-case of SSE) *Let Δ and ϵ satisfy IQC(Ψ, M) and the extended system $\Sigma_{e,x}$ of (31) is well-posed, if there exists a scalar $\lambda > 0$ and a continuously differentiable matrix $P = P^T$ with appropriate dimension such that $P \geq 0$ and for all $(s, \dot{s}) \in \Omega \times \dot{\mathcal{S}}$ (Omitting s and \dot{s} for a shorter notation):*

$$\begin{aligned} & \begin{bmatrix} PA + AP^T + \partial P & PB_1 & PB_2 \\ \mathcal{B}_1^T P & 0 & 0 \\ \mathcal{B}_2^T P & 0 & -I \end{bmatrix} \\ & + \lambda \begin{bmatrix} \mathcal{C}_1^T \\ \mathcal{D}_{11}^T \\ \mathcal{D}_{12}^T \end{bmatrix} M [\mathcal{C}_1 \quad \mathcal{D}_{11} \quad \mathcal{D}_{12}] < 0 \end{aligned} \quad (46)$$

and

$$\begin{bmatrix} P & \mathcal{C}_2^T \\ \mathcal{C}_2 & \sigma^2 I \end{bmatrix} > 0 \quad (47)$$

Then, the Supreme Square Error (SSE) satisfies:

$$\sup_{s \in \Omega} \sup_{0 \neq \eta \in \mathcal{L}_2, \zeta(0)=0} \left[\frac{\|y - \hat{y}\|_\infty}{\sqrt{\|y\|_2^2 + \|\hat{y}\|_2^2}} \right] < \sigma \quad (48)$$

Proof: Having the signals (χ, z, η, q, r) generated for the extended system given in 31 where we consider the input $\eta \in \mathcal{L}_2$ and parameter trajectory $s \in \Omega$ assuming zero initial conditions. Well-posedness assumption of the extended LPV system implies that all signals (χ, z, η, q, r) are well-defined. By assumption as well, the uncertainties Δ and ϵ satisfy the IQCs defined by (Ξ, M) and hence for any $T > 0$, the time domain expression of the IQCs in (18) must be satisfied by the signal r . Moreover, defining a storage function $V : \mathbb{R}^n \times \Omega \rightarrow \mathbb{R}_+$ by $V(\chi, s) = \chi^T P(s) \chi$. Also, the state space representation of the virtual filter (16) gives (36). Evaluating of the perturbed LMI (46) at $(s(t), \dot{s}(t))$ after multiplying its left/right by $[\chi^T, q^T, \eta^T]$ and $[\chi^T, q^T, x^T]^T$, respectively, yields the following dissipation inequality:

$$\nabla_\chi V \dot{\chi} + \nabla_s V \dot{s} \leq (1 - \epsilon) \eta \eta^T - \lambda r M r^T \quad (49)$$

This means that the dissipation inequality (49) is equivalent to the perturbed linear matrix inequality (46). Then, integrating along the state/parameter trajectory the obtained dissipation inequality (49) from lower bound $t = 0$ to upper bound $t = T$. Recalling that $\chi(0) = 0$, thus:

$$\begin{aligned} V(\chi(T), s(T)) \leq & (1 - \epsilon) \int_0^T \eta(\tau) \eta(\tau)^T d\tau \\ & - \lambda \int_0^T r(\tau) M r(\tau)^T d\tau \end{aligned} \quad (50)$$

It follows from the IQCs condition (18), that

$$V(\chi(T), s(T)) \leq (1 - \varepsilon) \int_0^T \eta(\tau)\eta(\tau)^T d\tau \quad (51)$$

Now, applying Schur complement on (47) and multiplying left and right by χ , z and its transpose χ^T , respectively, results:

$$\frac{1}{\sigma^2} z(t)z^T(t) \leq \chi^T(t)P(s)\chi(t) \quad \forall t > 0 \quad (52)$$

Evaluating (52) at $t = T$, and applying (51) yields:

$$\frac{1}{\sigma^2} z(T)z^T(T) \leq (1 - \varepsilon) \int_0^T \eta(\tau)\eta(\tau)^T d\tau \quad (53)$$

Knowing the $\varepsilon > 0$, therefore

$$\frac{1}{\sigma^2} z(T)z^T(T) \leq \int_0^T \eta(\tau)\eta(\tau)^T d\tau \quad (54)$$

Considering the supremum over T to demonstrate that $\|z\|_\infty \leq \sigma\|\eta\|_2$. Knowing that this result holds for any given input $\eta \in \mathcal{L}_2$, admissible trajectory solution $s \in \Omega$, and uncertainty $\Delta, \epsilon \in IQC(\Xi, M)$. Thus,

$$\sup_{s \in \Omega} \sup_{0 \neq \eta \in \mathcal{L}_2, \zeta(0)=0} \frac{\|z(t)\|_\infty}{\|\eta(t)\|_2} < \sigma \quad (55)$$

Having $\|z(t)\|_\infty = \|y(t) - \hat{y}(t)\|_\infty$ and $\|\eta(t)\|_2 = \sqrt{\|y(t)\|_2^2 + \|\hat{y}(t)\|_2^2}$, this implies

$$\frac{\|z(t)\|_\infty}{\|\eta(t)\|_2} = \frac{\|y - \hat{y}\|_\infty}{\sqrt{\|y\|_2^2 + \|\hat{y}\|_2^2}} \quad (56)$$

□ Theorem 2 is very important as it provides the maximum deviation expected of the closed-loop system with a NN controller from the closed-loop reference model. Having such information will give the user confidence to implement the NN controller by making the dynamical error small to insure the best performance possible. This worst case of SSE is a good indicator of the occurrence likelihood of any undesirable behavior in the closed-loop system when adopting the designed NN controller.

4 Validation and Numerical Simulation

In order to validate the theoretical results we have proved in the previous section, we will conduct tests using two different problems. Our first problem involves controlling a robot arm with only a single output, called the Single-Link Robot Arm Control Problem. A simpler and more focused scenario will allow us to evaluate the effectiveness of our approach.

Further, we will also test our approach on the more complex problem of Deep Guidance and Control of Apollo Lander, which involves multiple outputs. During the descent and landing phase of the Apollo Lander, precise control and guidance is required. We can further evaluate the robustness and adaptability of our approach by examining this more complex scenario with multiple outputs.

We notice here that the property of the activation function of the controller in quantity $\Lambda(s)$ allows us to express the set of a bounded convex domain \mathcal{G}_m^n of the matrix $\Lambda(s)$ as follows:

$$\mathcal{G}_m^n = \left\{ a_{ij} \leq \frac{\partial \pi_i}{\partial y_j} \leq b_{ij}, i = 1, \dots, n, j = 1, \dots, m \right\} \text{ and the set of vertices is defined by} \quad (57)$$

$$\mathcal{V}_{\mathcal{G}_m^n} = \{ \mathcal{V} = [\mathcal{V}_{11}, \dots, \mathcal{V}_{1m}, \dots, \mathcal{V}_{nm}] : \mathcal{V}_{ij} \in \{a_{ij}, b_{ij}\} \}$$

Also, IQCs provides a tool to study the stability of feedback connections of stable LTI systems and perturbation blocks as shown in Fig. 2. IQCs corresponding to many perturbation blocks is already available in the literature. Furthermore, a MATLAB toolbox for IQC-based stability and performance analysis exists and is called IQC- β . For different perturbations, different multipliers, e.g. constant or frequency dependent, are necessary to lead to non-conservative analysis and design results. Within IQC- β toolbox the different multipliers are chosen automatically

for user's convenience. As the dissipation inequality (38) is equivalent to the perturbed linear matrix inequality (33), the user, in IQC- β toolbox, has only to choose the type of IQC, which is more physically related, e.g. LTI uncertain parameter [Jonsson et al., 2004].

Since the modelling open source toolbox IQC- β we are using in this work does not support LPV formulation, the source of parameters variation, represented by the matrix $\Lambda(s)$, will therefore be modelled using the vertices defined in (57). More information can be found in [Boyd and Vandenberghe, 2001].

4.1 Single-Link Robot Arm Control Problem

4.1.1 Step 1: Problem Setting

The simulation validation that we conduct in this section uses the worst-case of RISE metric resulting from Theorem 1 since the open source tool we adopt for simulation calculations can only provide \mathcal{L}_2 to \mathcal{L}_2 gain.

Consider the nonlinear single-link robot arm example, shown in Fig. 3, with parameters $m = 0.15kg$, length $l = 0.5m$, and friction coefficient $\mu = 0.5Nms/rad$. The state space representation of the arm's motion is given by:

$$\begin{cases} \dot{\omega}(t) &= -10 \sin(\theta(t)) - 2\omega(t) + \tau(t) \\ \dot{\theta}(t) &= \omega(t) \end{cases} \quad (58)$$

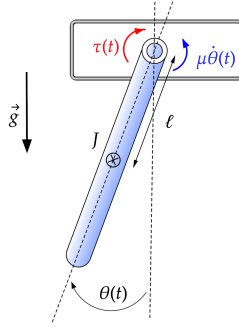


Figure 3: Single-link robot arm.

4.1.2 Step 2: Linear Reference Model

We start by training a neural controller with the aim that the arm with this neural controller tracks the closed-loop reference model given by:

$$\begin{cases} \dot{\omega}_r(t) &= -9\theta_r(t) - 6\omega_r(t) + 9r(t) \\ \dot{\theta}_r(t) &= \omega_r(t) \end{cases} \quad (59)$$

This means that the dynamic behavior of the system (58) in the closed-loop system after the training of the neural controller is close to the desired closed loop dynamics (59). The ideal case is when the system with a NN controller (58) matches the closed loop reference model (59) at all time t . However, this is nearly impossible in practice. The objective of this example is to determine the worst relative squared difference, γ , between the robot arm with neural control system closing the loop, while subject to its nonlinear functions, and the ideal closed loop reference model, where

$$\sup_{s \in \Omega} \sup_{0 \neq [\theta(t) \ \theta_r(t)]^T \in \mathcal{L}_2, \zeta(0)=0} \frac{\|\theta(t) - \theta_r(t)\|_2}{\|[\theta^T(t) \ \theta_r^T(t)]^T\|_2} < \gamma \quad (60)$$

To this end, let assume the static non-linearity $\Delta(\theta) = \theta - \sin(\theta)$ which is slope-restricted and sector bounded. We rearrange (58) then into the form:

$$\begin{cases} \dot{\omega}(t) &= -9\theta(t) - 2\omega(t) + \tau(t) + 10q(t) \\ \dot{\theta}(t) &= \omega(t), \quad p(t) = \theta(t) \\ \Delta(\theta) &= q(t) = \theta - \sin(\theta) \end{cases} \quad (61)$$

4.1.3 Step 3: Error Dynamical System

Now, we generate the error dynamical system using the closed loop reference model (59) and the new mathematical form of the arm's motion (61). Let $\delta\omega = \omega - \omega_r$, $\delta\theta = \theta - \theta_r$ and $\delta\tau = \tau - \tau_r$ then

$$\frac{d}{dt} \begin{bmatrix} \delta\omega \\ \delta\theta \end{bmatrix} = \begin{bmatrix} -6 & -9 \\ 1 & 0 \end{bmatrix} \begin{bmatrix} \delta\omega \\ \delta\theta \end{bmatrix} + \begin{bmatrix} 10 \\ 0 \end{bmatrix} q(t) + \begin{bmatrix} 1 \\ 0 \end{bmatrix} \delta\tau(t) \quad (62)$$

where $\tau_r(t) = \pi^*(\theta, t)$ and

$$\pi^*(\theta, t) = 10\theta_r(t) + 4\omega_r(t) - 9r(t) - 10\sin(\theta_r(t)) \quad (63)$$

The Neural controller architecture adopted in this example is given in Fig. 4. The output of the neural controller is given by :

$$\pi(\theta, t) = w_4 \tanh(w_1\theta(t) + w_2r(t) + w_3\pi(\theta(t)) + b_1) + b_2 \quad (64)$$

where $\tau(t) = \pi(\theta, t)$.

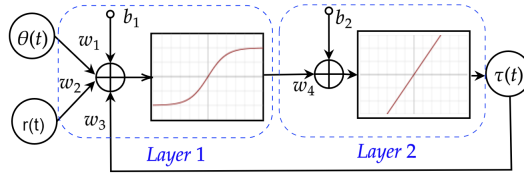


Figure 4: Neural controller π^* architecture.

Differential Mean Value Theorem [Zemouche et al., 2005] introduced in lemma 1, can convert the dynamical error system to an LPV system without nonlinearities of the neural controller. According to lemma 2, the approximation error $\delta\tau(t) = \mu(t)$ given in (11) can be expressed as :

$$\delta\tau(t) = \mu(t) = \Lambda(s)C\zeta(t) + \Lambda(s)D_p\Delta(y(t)) + \epsilon(\hat{y}(t)) \quad (65)$$

and the vectors $s_1, \dots, s_n \in \mathbf{Co}(y(t), \hat{y}(t))$, $s_i \neq y_1$, $s_i \neq y_2$, $i = 1, \dots, n$ such that

$$\Lambda(s) = \sum_{i=1}^m \sum_{j=1}^n e_m(i) e_n^T(j) \frac{\partial \pi_i}{\partial y_j}(s_i)$$

where

$$\epsilon(\hat{y}(t)) = \pi(\hat{y}(t)) - \pi^*(\hat{y}(t), t)$$

In this case, we have $C = [0 \ 1]$, $\zeta(t) = [\delta\omega(t) \ \delta\theta(t)]^T$, $D_p = 0$, $\hat{y}(t) = \theta_r$ and $y(t) = \theta(t)$. Therefore,

$$\delta\tau(t) = \Lambda(s)\delta\theta(t) + \epsilon(\theta_r(t)) \quad (66)$$

4.1.4 Step 4: Characterisation of the nonlinearities Δ and ϵ using IQCs

To choose the type of IQCs of the uncertainties considered for this simulation example, let us start with the static non-linearity $\Delta(\theta) = \theta - \sin(\theta)$. It is clear from the drawn figure Fig. 5 that the uncertainty $\Delta(\theta)$ is slope-restricted and sector bounded. Fig. 5 provides the IQCs characterisation of this non-linearity and plots the graph $\Delta = f(\theta)$ where $\Delta(\theta(t)) = \varphi(\theta, t)$ and $\alpha\theta(t) \leq \varphi(\theta, t) \leq \beta\theta(t)$ for all $\theta \in [-\frac{\pi}{2}, \frac{\pi}{2}]$. Simple calculation of the slope gives $\alpha = 0$ and $\beta = 0.364$ representing the bounds of the uncertainty Δ .

Similarly, we have the nonlinearity $\epsilon(\theta_r) = \pi(\theta_r) - \pi^*(\theta_r)$, where π^* and π are given in (63) and (64), respectively. The graph of $\epsilon = \hat{f}(\theta_r)$ is shown in Fig 6 where $\epsilon(\theta_r(t)) = \varrho(\theta_r, t)$ and $|\varrho(\theta_r, t)| \leq 0.2$ for all $\theta_r \in [-\frac{\pi}{2}, \frac{\pi}{2}]$. The IQCs characterisation of this nonlinearity is thus conducted as we show in Fig 6 that it is bounded by 0.2 and -0.2.

4.1.5 Step 5: IQCs based analysis results

Now, we would like to compute an upper bound on the \mathcal{L}_2 -gain from the output error $\theta - \theta_r$ to the outputs vector $[\theta, \theta_r]$. We use IQC- β toolbox to express and formulate the \mathcal{L}_2 gain estimation problem. Fig. 7 explains how to adapt our case to MATLAB IQCs- β Toolbox. We only need the two linear systems, the closed loop reference model and the

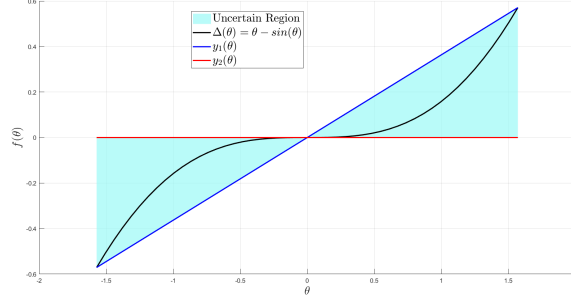


Figure 5: IQCs characterisation of the non-linearity Δ .

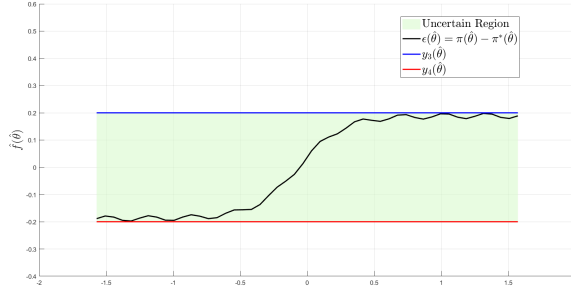


Figure 6: IQCs characterisation of the non-linearity ϵ .

dynamical error system, since the output of the closed-loop system with the NN controller is the sum of the outputs of the those two systems. The bounds of the uncertainty Δ and the nonlinearity ϵ derived in the previous sub-section are also provided as inputs to the IQCs- β Toolbox.

According to the results given by IQCs- β for the model in Fig.8 corresponding to the original Single-Link Robot Arm Control Problem:

$$\sup_{s \in \Omega} \sup_{0 \neq [\theta(t) \ \theta_r(t)]^T \in \mathcal{L}_2, \zeta(0)=0} \frac{\|\theta(t) - \theta_r(t)\|_2}{\|[\theta^T(t) \ \theta_r^T(t)]^T\|_2} < \gamma = 0.05669 \quad (67)$$

γ is the worst case of the mean integrated squared error between the closed loop system with the trained neural controller and the closed loop reference system and is less than 5.669%. According to [Atkins et al., 2013], the time Integral of the Square of the Error (ISE) in a control system is used as a measure of the performance of the system.

The value of γ represents the worst case of the relative error between the closed loop reference model, used for collecting data to train the NN controller, and the uncertain system with the designed neural controller.

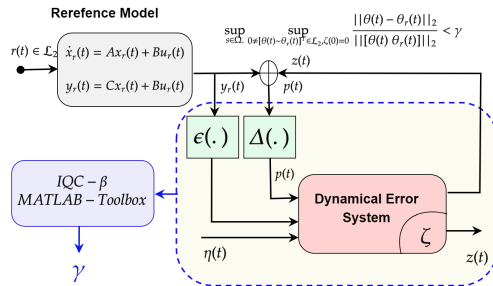


Figure 7: Adaption of IQCs- β MATLAB tool for the problem.

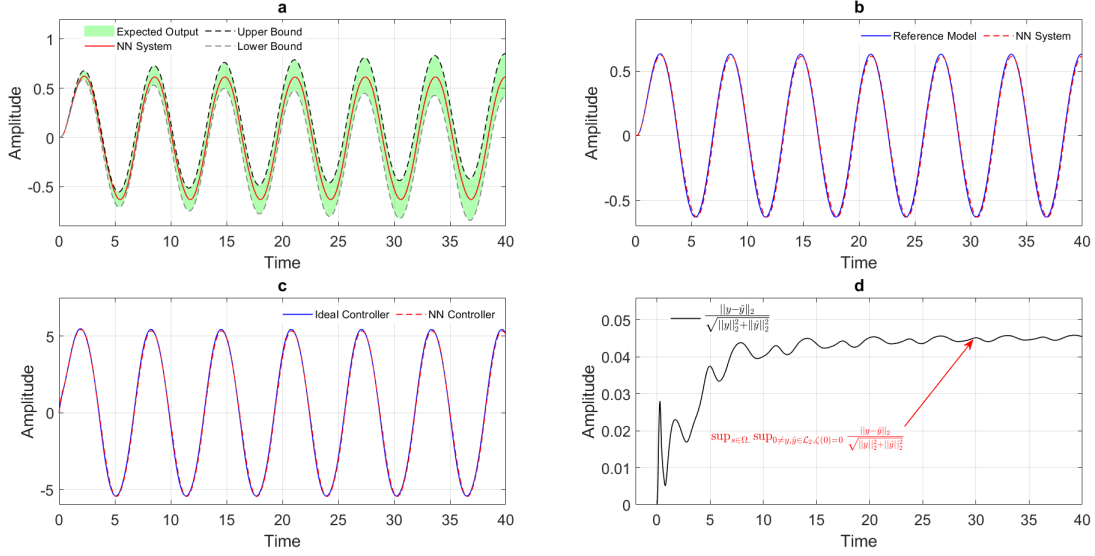


Figure 8: **Case Study A:** (a) Plot for the closed-loop system with the NN within the region of expectation (b) Plot of the output of reference model response θ_r , indicated in blue and the one of the closed-loop uncertain robotic arm system with neural controller θ indicated in red. (c) The controllers π and π^* outputs. (d) The relative squared difference between the robot arm neural control system is subject to uncertainty in nonlinear functions and the reference model.

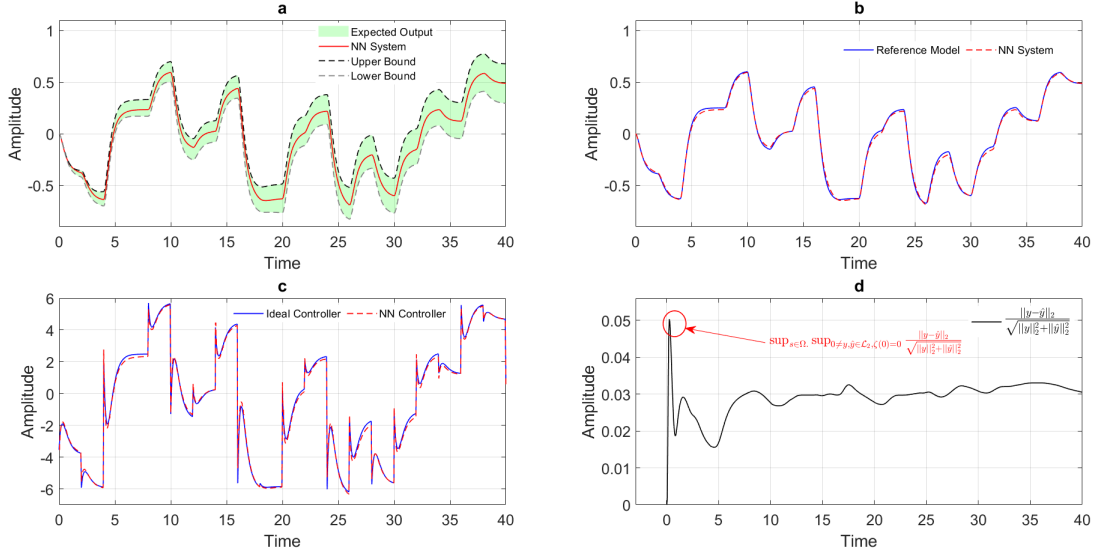


Figure 9: **Case Study B:** (a) Plot for the closed-loop system with the NN within the region of expectation (b) Plot of the output of reference model response θ_r , indicated in blue and the one of the closed-loop uncertain robotic arm system with neural controller θ indicated in red. (c) The controllers π and π^* outputs. (d) Relative squared difference between the robot arm neural control system subject to uncertainty in nonlinear functions and the reference model.

This worst-case result can be used to improve the robustness of the NN controller by making the dynamical error smaller which in turn will guarantee a better performance of the NN controller when it is implemented. This worst-case measure is also an indication of the appearance likelihood of any undesirable behavior in the closed loop system when adopting the designed NN controller.

To illustrate further the results of our controlled Single-Link Robot Arm with our designed neural controller, we propose two study cases: A and B. The reference of the first case study is periodically applied to the uncertain system with a neural controller and the reference closed-loop model. Using the equation given in (35), we can plot the expected region by utilise the information about the worst-case of the error and the known linear reference model as follow:

$$\|\theta(t) - \theta_r(t)\|_2 < \frac{2\gamma}{1-\gamma} \|\theta_r(t)\|_2 = 0.1202 \|\theta_r(t)\|_2 \quad (68)$$

Fig. 8 shows in sub-figure (a) the response of the system with the trained NN controller and clearly, the output remains inside the expected bound region. In sub-figure (b) of Fig. 8, the two responses (i.e. closed loop reference model and the uncertain plant with NN controller) for this first case study are shown. We can see from this figure that the uncertain plant with NN controller keeps close to the response of the closed-loop reference model. The neural controller output is also very close to the output of the reference controller used in the reference closed-loop model as shown in sub-figure (c) of Fig. 8. Moreover, we can see in sub-figure (d) of Fig. 8 that the value of $\frac{\|\theta(t) - \theta_r(t)\|_2}{\|[\theta^T(t) \ \theta_r^T(t)]^T\|_2}$ reaches the maximum of 0.045 approximately which is less than the worst-case $\gamma = 0.05669$. The same thing said above for the sub-figures of Fig. 8 can be said regarding the non-periodic case study B illustrated in the sub-figures of Fig 9 where the value $\frac{\|\theta(t) - \theta_r(t)\|_2}{\|[\theta^T(t) \ \theta_r^T(t)]^T\|_2}$ has a maximum pic of around 0.051 which is less than the worst case γ as well and the response of the system with NN controller is always inside the region of performance expectation.

4.2 Deep Guidance and Control of Apollo Lander

In the classical Guidance and Control of Apollo Lander described in [Amaral, 2019], GC system generates trajectory and thrust commands to manoeuvre the lander for a given initial position, velocity, and desired landing target. The control part is compensated for by the Martian atmosphere and converted into inertial coordinates before the position commander uses the information [Millour et al., 2015].

4.2.1 Step 1: Problem Setting

We perform the test of the trained network in closed-loop using the parameters listed in Table 1 with the aim of validating its performance. In terms of applying aerodynamic forces and torques which are external disturbances on the lander, coefficient of drag C_D is 2.0, and it is assumed to be constant, whereas surface-relative head wind is in the range of $20m/s$. Furthermore, the air density ρ is assumed to be $0.023kg/m^3$ throughout. Under this scenario, the worst-case aerodynamic resistance during the descent phase is less than 2% of the vehicle's maximum thrust. Due to the close-loop control action, aerodynamic forces and torques are automatically compensated.

Table 1: Simulation Parameters

Parameter	value
Initial Position p_0 [m]	$[-5632.2, 709.25, 6190.5]^T$
Initial Velocity v_0 [m/s]	$[206.48, -26.006, -103.51]^T$
Initial Acceleration a_0 [m/s ²]	$[-2.1124, 0.24947, -2.6404]^T$
Initial Mass m_0 [Kg]	600.3
The capsule reference area S	5.137426149499100
Mars Gravity g [m/s ²]	$[0, 0, 3.725258]^T$
Engine Maximum Thrust T [N]	3600
Maximum Throttle Level T_{max}	100%
Minimum Throttle Level T_{min}	30%

Atmosphere As part of the Mars environment module, the horizontal wind is included in the atmospheric model. Based on lookup tables, an atmospheric model specifies the properties of the Martian atmosphere at a specific location. The atmospheric properties are obtained directly from the Mars Climate Database (MCD) v.5.2 at the mission's specified landing coordinates. MCD is derived from numerical simulations of the Martian atmosphere using General Circulation Models (GCM) and validated by observations of the Martian atmosphere. For more details see [Millour et al., 2015].

Lander Dynamics In closed-loop simulations, Newton's second law is used to model a point mass's robotic lander motion, where the lander motion is expressed in the LENU frame as follow:

$$\frac{d[r]_{LENU}}{dt} = [v]_{LENU}, \quad (69)$$

where $([v]_{LENU})$ refer to the relative velocity of the robotic lander. In in the LENU frame and the lander mass (m), The dynamics equation is given based on the force resultant $([F]_{LENU})$ expressed as:

$$\frac{d[v]_{LENU}}{dt} = [a]_{LENU} = \frac{[F]_{LENU}}{m}. \quad (70)$$

Aerodynamics In the simulations, a lookup table is used as the aerodynamics model of the Apollo capsule. In this module, only aerodynamic drag forces are considered following equation:

$$F_D = \frac{1}{2} \rho v^2 C_D (\text{Ma}) S, \quad (71)$$

where ρ represents the atmosphere density, C_D denotes the capsule drag coefficient as a function of the Mach number (Ma), the capsule reference area represented by the S , and v is the capsule velocity relative to the fluid velocity expressed in the landing site East-North-UP frame.

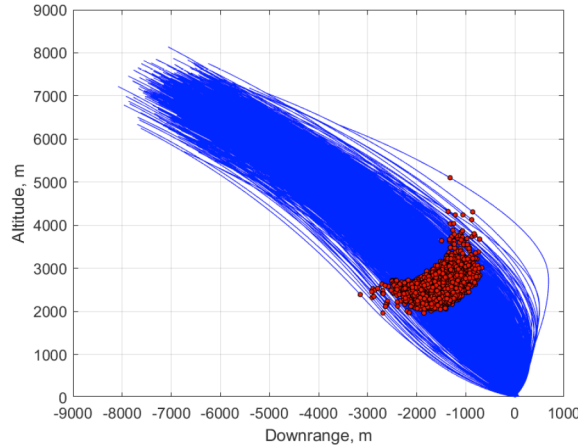


Figure 10: Plot of the 1537 trajectories [Amaral, 2019]. The marked dots representing the trigger locations. An optimal altitude to trigger is in the range of 2 km to 3 km, and in some trajectories, overshooting the target is the best behavior.

Actuators In the actuator model, four thrusters engines are used to generate forces concerning the center of mass of the vehicle. The main engine responsible on the force F_{Thr} is located along with the vehicle z -axis, while the remaining are the sources of saturated forces F_{Trq} are placed at a distance l from the mass center to generate pure torques along positive and negative axes. To calculate the fuel consumption, the mass flow rate is integrated:

$$\dot{m}_{fuel} = V_e^{-1} \left(F_{Thr} + \sum F_{Trq} \right), \quad (72)$$

where $V_e = g_0 I_{sp}$.

Apollo Guidance The algorithm is based on the idea of following the reference trajectory backwards in time from the target point to the present moment. The time-to-go (t_{go}), represents the time left until the desired landing is reached, so it tends to zero as time gets closer to the goal. In [Klumpp, 1974], the reference trajectory satisfies a two-boundary problem with five degrees of freedom. Accordingly, the reference trajectory must be a polynomial function of fourth or higher order. Therefore, the reference position (r_d given at t_{go} as a function of the target state as:

$$r_d = r_t + v_t t_{go} + a_t \frac{t_{go}^2}{2} + j_t \frac{t_{go}^3}{6} + s_t \frac{t_{go}^4}{24}, \quad (73)$$

where r_t refers to the target position, v_t represents the target velocity and a_t, j_t, s_t denote the target acceleration, jerk and snap, respectively.

According to (73), the work of [Huang et al., 2022] describes the acceleration command (a_{cmd}) as a quadratic polynomial i.e.

$$a_{cmd} = C_0 + C_1 t_{go} + C_2 t_{go}^2. \quad (74)$$

The coefficients of the polynomial are derived by solving a system of three equations comprising (74). The two other equations related to the target velocity and position equations are obtained by by integrating the target acceleration equation:

$$\begin{cases} a_t = C_0 + C_1 t_{go} + C_2 t_{go}^2 \\ v_t = C_0 t_{go} + \frac{1}{2} C_1 t_{go}^2 + \frac{1}{3} C_2 t_{go}^3 + v \\ r_t = v t_{go} + \frac{1}{2} C_0 t_{go}^2 + \frac{1}{6} C_1 t_{go}^3 + \frac{1}{12} C_2 t_{go}^4 + r \end{cases} \quad (75)$$

where a_t represents the reference acceleration vector, r and v denote the vehicle current position and velocity, respectively. The following values for the polynomial coefficients (C_0 , C_1 and C_2) are obtained by solving the following matrix system:

$$\begin{bmatrix} a_t \\ v_t \\ r_t \end{bmatrix} = \begin{bmatrix} 1 & t_{go} & t_{go}^2 \\ t_{go} & \frac{1}{2} t_{go}^2 & \frac{1}{3} t_{go}^3 \\ \frac{1}{2} t_{go}^2 & \frac{1}{6} t_{go}^3 & \frac{1}{12} t_{go}^4 \end{bmatrix} \begin{bmatrix} C_0 \\ C_1 \\ C_2 \end{bmatrix} + \begin{bmatrix} 0 \\ v \\ v t_{go} \end{bmatrix}. \quad (76)$$

Therefore,

$$\begin{cases} C_0 = a_t - 6 \left(\frac{v_t + v}{t_{go}} \right) + 12 \left(\frac{r_t - r}{t_{go}^2} \right) \\ C_1 = -6 \left(\frac{a_t}{t_{go}} \right) + 6 \left(\frac{5v_t + 3v}{t_{go}^2} \right) - 48 \left(\frac{r_t - r}{t_{go}^3} \right) \\ C_2 = 6 \left(\frac{a_t}{t_{go}^2} \right) - 12 \left(\frac{2v_t + v}{t_{go}^3} \right) + 36 \left(\frac{r_t - r}{t_{go}^4} \right) \end{cases} \quad (77)$$

By defining the vertical component of the acceleration profile as a linear function of t_{go} . Hence, solving (74) for t_{go} two solutions are obtained:

$$\begin{aligned} & \text{If } |(a_t)_z| > 0 \\ & t_{go} = \frac{2(v_t)_z + (v)_z}{(a_t)_z} + \sqrt{\left[\frac{2(v_t)_z + (v)_z}{(a_t)_z} \right]^2 + \frac{6[(r_t)_z - (r)_z]}{(a_t)_z}}, \\ & \text{else if } (a_t)_z = 0 \\ & t_{go} = \frac{3[(r_t)_z - (r)_z]}{(v)_z + 2(v_t)_z}, \end{aligned} \quad (78)$$

where $(\cdot)_z$ denotes the vertical component of the variable (\cdot)

A robustness analysis of feedback systems Apollo lander based on NN controllers against potential uncertainties is presented here. To achieve this, we need to follow the below pattern where we aiming at keeping the output of the closed-loop system with a NN controller close to the output of an ideal and trusted closed-loop reference model when its input changes within a bounded set.

4.2.2 Step 2: Linear Reference Model

We start by training a neural controller with the aim that the lander system with this neural controller tracks classical Apollo controller provided in [Amaral, 2019]. A linear reference model is what we want. To generate the linear closed-loop reference model, we use the Five Tau rule, which states that transient events die down after five Tau seconds. In other words, a transition from a (steady) state to another (steady) state lasts only for five Tau seconds. Let consider the following form of the reference model:

$$\begin{bmatrix} \frac{dx}{dt} \\ \frac{dv}{dt} \end{bmatrix} = \begin{bmatrix} \hat{v}(t) \\ a\hat{v}(t) + \hat{u}(t) \end{bmatrix} \quad (79)$$

where

$$a = \begin{pmatrix} a_x & 0 & 0 \\ 0 & a_y & 0 \\ 0 & 0 & a_z \end{pmatrix}$$

MATLAB is used to find the matrix a using regression linear technique:

$$a = \arg \min_v \left(\frac{1}{2} \frac{\rho}{m} v^2 C_D (\text{Ma}) S - av(t) \right) \quad (80)$$

As a result, we obtain the matrix a as follows:

$$a = \begin{pmatrix} -0.0087 & 0 & 0 \\ 0 & -0.0075 & 0 \\ 0 & 0 & -0.0077 \end{pmatrix} \quad (81)$$

The linear reference model is now complete, and we can move on to finding the best controller which has dynamical behaviour too close to the nonlinear classical one. MATLAB is used to implement the poles placement technique (state feedback control) along with Five Tau rule. The linear closed-loop reference model and the nonlinear classical Apollo are compared via simulation for some scenarios to illustrate their close responses. Both systems have closed responses, as shown in Figure 11 and Figure 12.

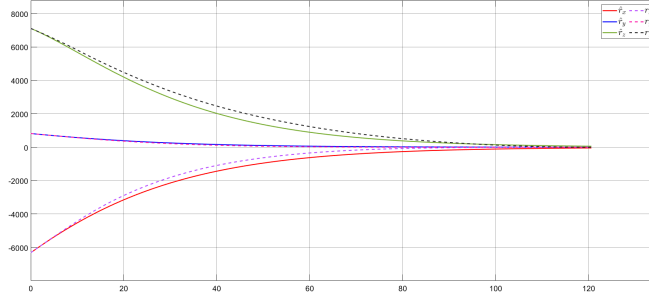


Figure 11: Position: linear reference model vs. the nonlinear Apollo Model.

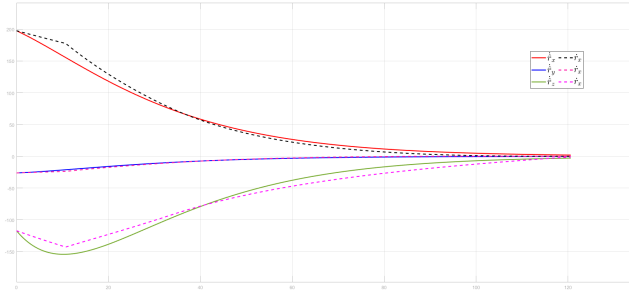


Figure 12: Velocity: linear reference model vs. the nonlinear Apollo .

The neural controller in TABLE 2 was trained with the aim that the lander dynamics with this neural controller tracks the closed-loop reference Apollo model. This means that the dynamic behaviour of the system in the closed-loop system after the training of the neural controller is close to the linear reference closed loop dynamics. In an ideal world, the closed loop Apollo model would be matched by the system with a NN controller at all times t . In reality, this is almost impossible. In this example, we are calculating the worst relative squared difference, γ , between the classical Apollo system provided in [Amaral, 2019] with neural control system closing the loop, while subject to its nonlinear functions, and the ideal closed loop reference model. For this purpose, let assume the static non-linearity $\Delta(v(t)) = \frac{1}{2} \frac{\rho}{m} v^2(t) C_D (\text{Ma}) S - av(t)$ which is slope-restricted, and sector bounded. The Lander dynamics are then rearranged into the following form:

$$\begin{cases} \begin{pmatrix} \frac{dr}{dt} \\ \frac{dv}{dt} \end{pmatrix} = \begin{bmatrix} v \\ av(t) + u(t) + \Delta(v(t)) \end{bmatrix} \\ \Delta(v(t)) = \frac{1}{2} \frac{\rho}{m} v^2(t) C_D (\text{Ma}) S - av(t) \\ y(t) = \begin{pmatrix} r(t) \\ v(t) \end{pmatrix} \end{cases} \quad (82)$$

Table 2: Neural Controller Architecture

Layer	No. Neurons/Activation Function
Input layer	6/ Linear $[r^T(t), v^T(t)]^T$
1 st layer	40/Tanh
2 nd layer	40/Sigmoid
3 rd layer	40/Tanh
Output layer	3/ Linear

4.2.3 Step 3: Error Dynamical System

By using the closed loop reference model and the new mathematical form of the Lander dynamical motion, we can now construct the error dynamical system. Let $\delta r = r - \hat{r}$, $\delta v = v - \hat{v}$ and $\delta u = u - \hat{u}$ then

$$\begin{cases} \left(\begin{array}{c} \frac{d\delta r}{dt} \\ \frac{d\delta v}{dt} \end{array} \right) = \begin{bmatrix} \delta v \\ a\delta v(t) + \delta u(t) + \Delta(v(t)) \end{bmatrix} \\ \Delta(v(t)) = \frac{1}{2} \frac{\rho}{m} v^2(t) C_D (\text{Ma}) S - av(t) \\ z(t) = \begin{pmatrix} \delta r(t) \\ \delta v(t) \end{pmatrix} \end{cases} \quad (83)$$

According to lemma 2, the approximation error $\delta u = u - \hat{u}$ given in the equation above can be expressed as:

$$\delta u(t) = \Lambda(s) \begin{pmatrix} \delta r(t) \\ \delta v(t) \end{pmatrix} + \epsilon(\hat{v}(t)) \quad (84)$$

where $\epsilon(\hat{v}(t)) = u(\hat{v}(t)) - \hat{u}(\hat{v}(t))$. Then, the dynamical error became:

$$\begin{cases} \left[\begin{array}{c} \frac{d\delta r}{dt} \\ \frac{d\delta v}{dt} \end{array} \right] = \begin{bmatrix} \delta v(t) \\ a\delta v(t) + \Delta(v(t)) \end{bmatrix} + B\Lambda(s) \begin{bmatrix} \delta r(t) \\ \delta v(t) \end{bmatrix} \\ \Delta(v(t)) = \frac{1}{2} \frac{\rho}{m} v^2(t) C_D (\text{Ma}) S - av(t) \\ z(t) = \begin{pmatrix} \delta r(t) \\ \delta v(t) \end{pmatrix}, \quad B = \begin{bmatrix} 0 & 0 & 0 \\ 0 & 0 & 0 \\ 0 & 0 & 0 \\ 1 & 0 & 0 \\ 0 & 1 & 0 \\ 0 & 0 & 1 \end{bmatrix} \end{cases} \quad (85)$$

4.2.4 Step 4: IQCs Characterisation of the nonlinearities Δ and ϵ

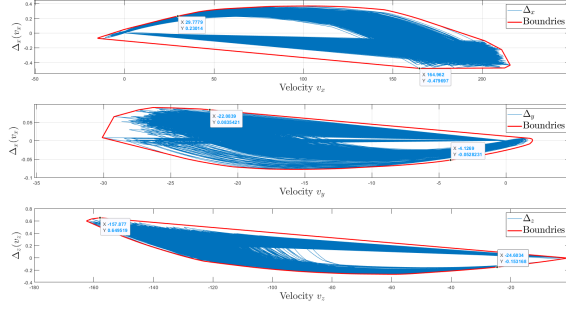
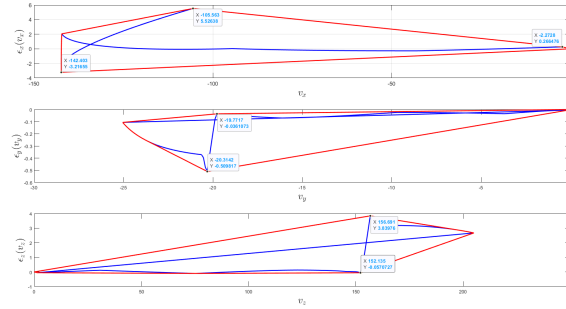
To choose the type of IQCs of the uncertainties considered for this example, let start with the static non-linearity $\Delta(v(t)) = \frac{1}{2} \frac{\rho}{m} v^2(t) C_D (\text{Ma}) S - av(t)$. It is clear from the drawn Figure 13 that the uncertainty $\Delta(v(t))$ is slope-restricted and sector bounded. Figure 13 provides the IQCs characterisation of this non-linearity and plots the graph $\Delta(v(t))$ where $\Delta(v(t)) = \varphi(v, t)$ and $\alpha v(t) \leq \varphi(v, t) \leq \beta v(t)$ for all v . Simple calculation of the slope gives $\alpha = [-0.003 \quad 0.013 \quad 0.006]^T$ and $\beta = [0.008 \quad -0.004 \quad -0.004]^T$ representing the bounds of the uncertainty Δ .

Similarly, we have the nonlinearity $\epsilon(\hat{v}(t)) = u(\hat{v}(t)) - \hat{u}(\hat{v}(t))$. The graph of $\epsilon = \hat{f}(\hat{v}(t))$ is shown in Figure 14 where $\hat{\alpha}\hat{v}(t) \leq \hat{f}(\hat{v}(t)) \leq \hat{\beta}\hat{v}(t)$. The IQCs characterisation of this nonlinearity is thus conducted to in $\hat{\beta} = [-0.052 \quad 0 \quad 0.0053]^T$ and $\hat{\alpha} = [0.022 \quad -0.024 \quad -0.0043]^T$.

4.2.5 Step 5: IQCs based Robustness Analysis Results

According to the results given by IQC- β for the model corresponding to the original Apollo Robustness Control Problem:

$$\begin{aligned} & \left[\begin{array}{cccccc} \frac{2\gamma_x}{1-\gamma_x} & \frac{2\gamma_y}{1-\gamma_y} & \frac{2\gamma_z}{1-\gamma_z} & \frac{2\gamma_{v_x}}{1-\gamma_{v_x}} & \frac{2\gamma_{v_y}}{1-\gamma_{v_y}} & \frac{2\gamma_{v_z}}{1-\gamma_{v_z}} \end{array} \right]^T \\ & = [0.0988 \quad 0.1992 \quad 0.1581 \quad 0.0119 \quad 0.0244 \quad 0.0158]^T \end{aligned}$$

Figure 13: IQCs characterisation of the non-linearity Δ .Figure 14: IQCs characterisation of the non-linearity ϵ .

The worst relative error between the closed loop system with the trained neural controller and the closed loop reference system and is less than $[9.88\% \ 19.92\% \ 15.81\% \ 1.19\% \ 2.44\% \ 1.58\%]^T$ of the reference model outputs. To illustrate further the results of our controlled Lander with our designed neural controller, we perform some simulation results. Figure 15 and Figure 16 show the response of the system with the trained NN controller for different two scenarios with different initial position and velocity. Clearly, the output remains inside the expected bound region.

Clearly, the novel approach results can be used to improve the robustness of the NN controller by making the dynamical error smaller which in turn will guarantee a better performance of the NN controller when it is implemented. The worst-case measure estimated here is also an indication of the appearance likelihood of any undesirable behaviour in the closed loop system when adopting the designed NN controller. The envelop can be reduced by using IQC toolbox that is compatible with LPV system also hybrid systems as we have discontinuity in the activation functions such Relu and Leaky-Relu which result in hybrid system case when we use the Jacobian of the system.

5 Conclusion

A novel technique named keep-close was presented to guarantee the safety and robustness of feedback systems with NN controllers against various uncertainty types. The theoretical results we reached for the worst-case analysis presented provides the user with a prior knowledge about the worst case of the error between the reference model and the state of the system with a neural controller including perturbations. The key idea of the new approach is to maintain the closed-loop system output with a NN controller when its input changes within a bounded set, close to the output of a robustly performing closed loop reference model. The keep-close approach provides the user a prior knowledge about the worst-case RISE and SSE between the reference closed-loop model and the uncertain system controlled by the neural controller. This information is very important to provide some levels of validation to AI-based ML techniques by using robust control theory and increasing the level of trust for users to adopt these schemes. Through the practical implementation and testing of two distinct problems, namely the Single-Link Robot Arm Control Problem and the Deep Guidance and Control of Apollo Lander, the theoretical results of the innovative approach presented in this paper have been successfully validated. These real-world experiments have substantiated the efficacy and adaptability of the

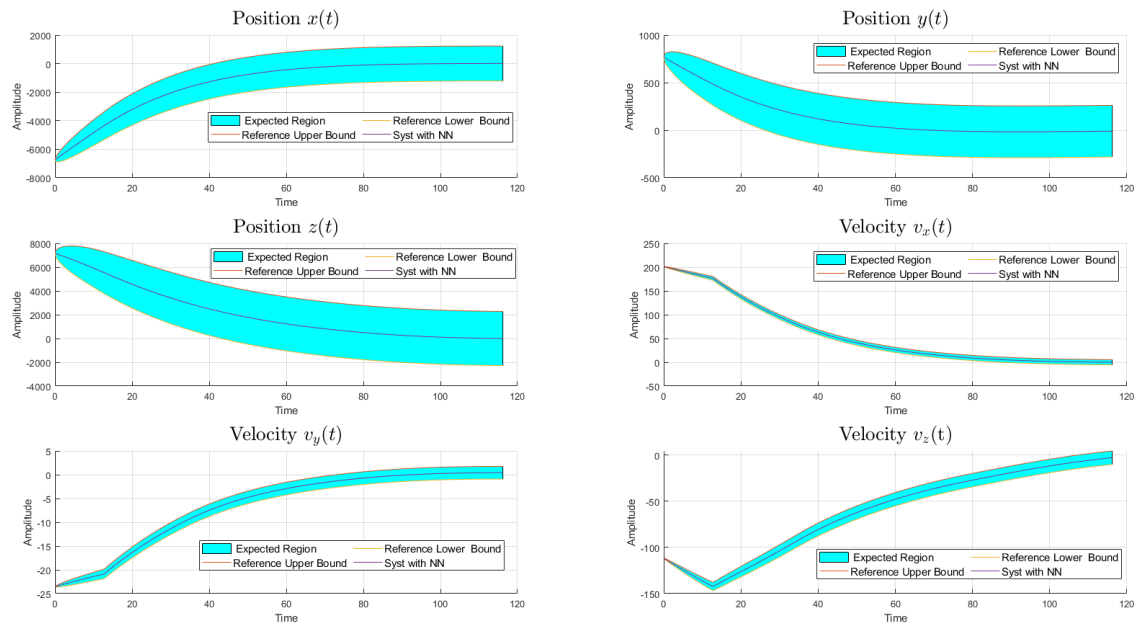


Figure 15: Simulation Results, Successful Landing Scenario.

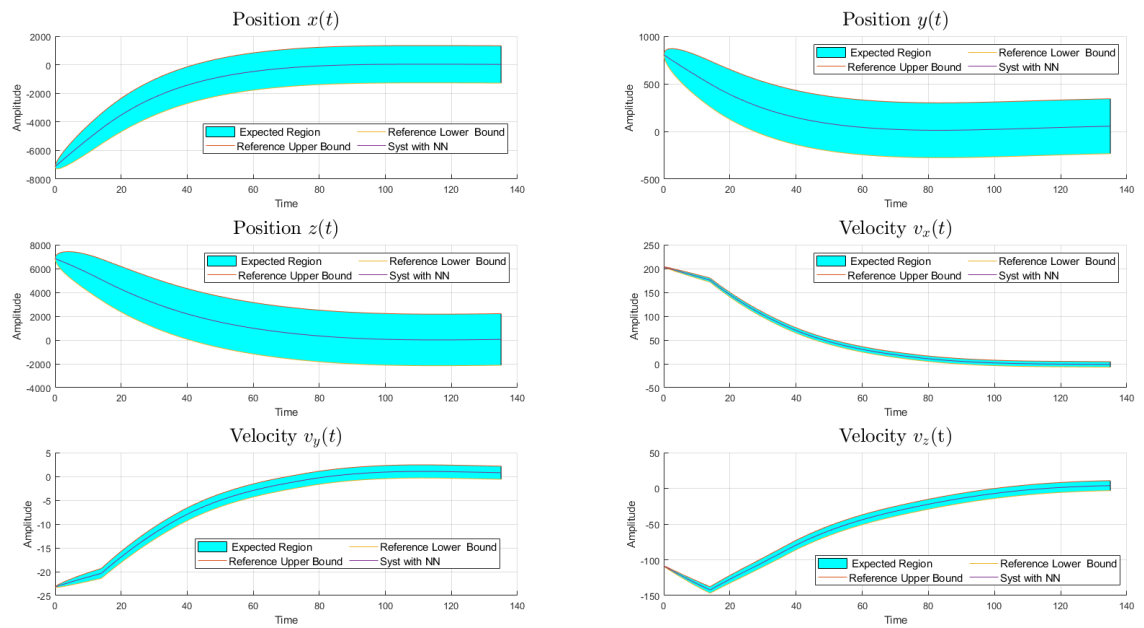


Figure 16: Simulation Results, Failed Landing Scenario.

proposed approach across diverse application domains, providing empirical evidence to support its effectiveness and versatility.

Acknowledgment

The authors would like to thank Spin-Works as a company and Tiago Amaral specifically for their software to generate data.

References

- Tiago Amaral. Guidance optimization for mars pinpoint landing with optimal trigger and re-optimization. 2019.
- Anthony G Atkins, Tony Atkins, and Marcel Escudier. *A dictionary of mechanical engineering*. Oxford University Press, 2013.
- S Boyd and L Vandenberghe. Convex optimization with engineering applications. *Lecture Notes, Stanford University, Stanford*, 2001.
- Shankar A Deka, Dušan M Stipanović, and Claire J Tomlin. Dynamically computing adversarial perturbations for recurrent neural networks. *IEEE Transactions on Control Systems Technology*, 2022.
- Abdelhafid Zenati et al. On the admissibility and stability of multi-agent nonlinear interconnected positive systems with heterogeneous delays. *IEEE Transactions on Automatic Control*, 2022.
- Haijun Fang, Zongli Lin, and Mario Rotea. On iqc approach to the analysis and design of linear systems subject to actuator saturation. *Systems & control letters*, 57(8):611–619, 2008.
- Mahyar Fazlyab, Manfred Morari, and George J Pappas. Safety verification and robustness analysis of neural networks via quadratic constraints and semidefinite programming. *IEEE Transactions on Automatic Control*, 2020.
- Matthias Fetzner, Carsten W Scherer, and Joost Veenman. Invariance with dynamic multipliers. *IEEE Transactions on Automatic Control*, 63(7):1929–1942, 2017.
- Xiangyu Huang, Chao Xu, Jinchang Hu, Maodeng Li, Minwen Guo, Xiaolei Wang, Yu Zhao, Baocheng Hua, and Yunpeng Wang. Powered-descent landing gnc system design and flight results for tianwen-1 mission. *Astrodynamics*, 6:3–16, 2022.
- Andrea Iannelli, Peter Seiler, and Andrés Marcos. Region of attraction analysis with integral quadratic constraints. *Automatica*, 109:108543, 2019.
- Radoslav Ivanov, Taylor J Carpenter, James Weimer, Rajeev Alur, George J Pappas, and Insup Lee. Verifying the safety of autonomous systems with neural network controllers. *ACM Transactions on Embedded Computing Systems (TECS)*, 20(1):1–26, 2020.
- Radoslav Ivanov, Taylor Carpenter, James Weimer, Rajeev Alur, George Pappas, and Insup Lee. Verisig 2.0: Verification of neural network controllers using taylor model preconditioning. In *International Conference on Computer Aided Verification*, pages 249–262. Springer, 2021.
- Ulf Jonsson, Chung-Yao Kao, Alexandre Megretski, and Anders Rantzer. A guide to iqc β : A matlab toolbox for robust stability and performance analysis. Technical report, Technical report, 2004. URL <http://www.ee.unimelb.edu.au/staff/cykao...>, 2004.
- SS Kelkar, LL Grigsby, and J Langsner. An extension of parseval’s theorem and its use in calculating transient energy in the frequency domain. *IEEE Transactions on Industrial Electronics*, 1(1):42–45, 1983.
- Hassan K Khalil. *Nonlinear control*, volume 406. Pearson New York, 2015.
- Allan R Klumpp. Apollo lunar descent guidance. *Automatica*, 10(2):133–146, 1974.
- Laurent Lessard, Benjamin Recht, and Andrew Packard. Analysis and design of optimization algorithms via integral quadratic constraints. *SIAM Journal on Optimization*, 26(1):57–95, 2016.
- Alexandre Megretski and Anders Rantzer. System analysis via integral quadratic constraints. *IEEE Transactions on Automatic Control*, 42(6):819–830, 1997.
- Ehouarn Millour, Francois Forget, Aymeric Spiga, T Navarro, Jean-Baptiste Madeleine, Luca Montabone, Alizée Pottier, Franck Lefevre, Franck Montmessin, Jean-Yves Chaufray, et al. The mars climate database (mcd version 5.2). In *European planetary science congress*, volume 10, pages 2015–2438, 2015.
- Phan Thanh Nam, Tran Ngoc Nguyen, Hieu Trinh, et al. Comparison principle for positive time-delay systems: An extension and its application. *Journal of the Franklin Institute*, 358(13):6818–6834, 2021.

- Patricia Pauli, Julian Berberich, and Frank Allgöwer. Robustness analysis and training of recurrent neural networks using dissipativity theory. *at-Automatisierungstechnik*, 70(8):730–739, 2022.
- Harald Pfifer and Peter Seiler. Robustness analysis of linear parameter varying systems using integral quadratic constraints. *International Journal of Robust and Nonlinear Control*, 25(15):2843–2864, 2015.
- Anders Rantzer. On the kalman-yakubovich-popov lemma for positive systems. *IEEE Transactions on Automatic Control*, 61(5):1346–1349, 2015.
- John Schulman, Sergey Levine, Pieter Abbeel, Michael Jordan, and Philipp Moritz. Trust region policy optimization. In *International conference on machine learning*, pages 1889–1897. PMLR, 2015.
- V Sharma, V Agrawal, BB Sharma, and R Nath. Unknown input nonlinear observer design for continuous and discrete time systems with input recovery scheme. *Nonlinear Dynamics*, 85:645–658, 2016.
- Erin Summers and Andrew Packard. L₂ gain verification for interconnections of locally stable systems using integral quadratic constraints. In *49th IEEE Conference on Decision and Control (CDC)*, pages 1460–1465. IEEE, 2010.
- Christian Szegedy, Wojciech Zaremba, Ilya Sutskever, Joan Bruna, Dumitru Erhan, Ian Goodfellow, and Rob Fergus. Intriguing properties of neural networks. *arXiv preprint arXiv:1312.6199*, 2013.
- Joost Veenman and Carsten W Scherer. Stability analysis with integral quadratic constraints: A dissipativity based proof. In *52nd IEEE Conference on Decision and Control*, pages 3770–3775. IEEE, 2013.
- Joost Veenman, Carsten W Scherer, and Hakan Köroğlu. Robust stability and performance analysis based on integral quadratic constraints. *European Journal of Control*, 31:1–32, 2016.
- Ruigang Wang and Ian R Manchester. Robust contraction analysis of nonlinear systems via differential iqc. In *2019 IEEE 58th Conference on Decision and Control (CDC)*, pages 6766–6771. IEEE, 2019.
- Weiming Xiang, Patrick Musau, Ayana A Wild, Diego Manzananas Lopez, Nathaniel Hamilton, Xiaodong Yang, Joel Rosenfeld, and Taylor T Johnson. Verification for machine learning, autonomy, and neural networks survey. *arXiv preprint arXiv:1810.01989*, 2018a.
- Weiming Xiang, Hoang-Dung Tran, Joel A Rosenfeld, and Taylor T Johnson. Reachable set estimation and safety verification for piecewise linear systems with neural network controllers. In *2018 Annual American Control Conference (ACC)*, pages 1574–1579. IEEE, 2018b.
- He Yin, Peter Seiler, and Murat Arcak. Stability analysis using quadratic constraints for systems with neural network controllers. *IEEE Transactions on Automatic Control*, 67(4):1980–1987, 2021a.
- He Yin, Peter Seiler, and Murat Arcak. Stability analysis using quadratic constraints for systems with neural network controllers. *IEEE Transactions on Automatic Control*, 67(4):1980–1987, 2021b.
- Ali Zemouche, Mohamed Boutayeb, and G Iulia Bara. Observer design for nonlinear systems: An approach based on the differential mean value theorem. In *Proceedings of the 44th IEEE Conference on Decision and Control*, pages 6353–6358. IEEE, 2005.
- Stephan Zheng, Yang Song, Thomas Leung, and Ian Goodfellow. Improving the robustness of deep neural networks via stability training. In *Proceedings of the IEEE conference on computer vision and pattern recognition*, pages 4480–4488, 2016.